

## Dynamics of self-replicating patterns in the one-dimensional Gray-Scott model

Daishin UYAMA

(Received March 5, 1998)

**Abstract.** We study the self-replicating pattern (SRP) that is observed in the one-dimensional Gray-Scott model from a global bifurcational view point. It is shown that the existence of the hierarchy structure of the limiting points of stationary Turing patterns causes SRP of static type as an aftereffect. The main difficulty lies in the fact that SRP is a real transient phenomenon and it can not be captured as an invariant set in a function space. The aftereffect is the reflection of the fact that each element of hierarchy structure is connected by unstable manifolds.

*Key words:* self-replicating pattern, reaction diffusion system, pulse solution, Turing pattern, wave splitting, Bogdanov-Takens point.

### 1. Introduction

The following Gray-Scott model attracts much attention recently by its variety of dynamics [1–8].

$$\begin{cases} \frac{\partial u}{\partial t} = D_u \nabla^2 u - uv^2 + F(1 - u) \\ \frac{\partial v}{\partial t} = D_v \nabla^2 v + uv^2 - (F + k)v. \end{cases} \quad (1)$$

Especially the self-replicating pattern depicted as in Figure 1.1 is one of the intriguing dynamics. It starts from a localized pulse and continues to split until the domain is filled by them completely. A similar type of replicating patterns has also been observed in a different model [12]. The main difficulty lies in the fact that SRP is a real transient phenomenon and it can not be captured as an invariant set in a function space. A new framework to understand such a transient behavior was proposed in [12] called the aftereffect of hierarchy structure of limiting points (AHL), however it is tough to show the existence of such a global structure even by numerics. The goal of this paper is to show that firstly the mechanism AHL

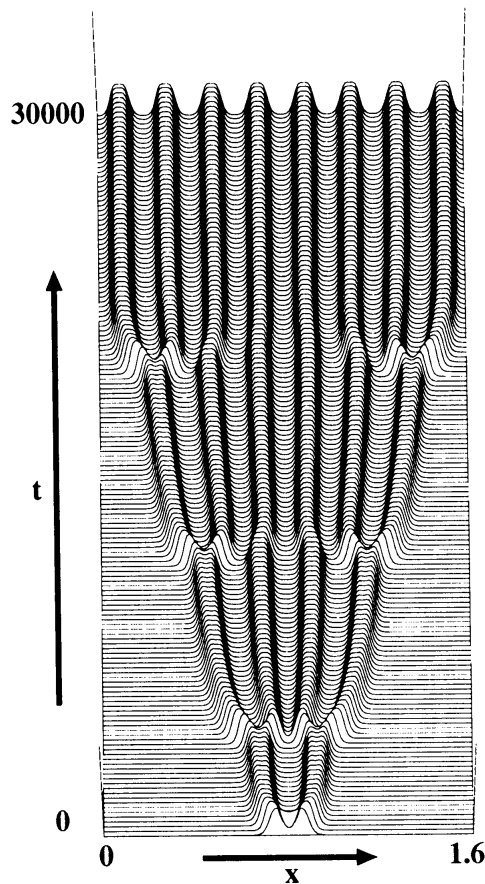


Fig. 1.1. A self-replicating pattern in the 1-dimensional Gray-Scott model (1) at  $F = 0.04$ ,  $k = 0.06075$ . The diffusion coefficients are  $D_u = 2 \times 10^{-5}$  and  $D_v = 10^{-5}$  respectively and the system size is 1.6. The boundary conditions is of Neumann type. The spatial mesh consisted of 1500 grid points. The figure displays the space-time profile of  $v$ .

proposed in [12] is really built in the Gray-Scott model, secondly there are two different types of self-replicating pattern, namely SRP of propagating type and of static type. In [12] the propagating type was discussed. We mainly focus on SRP of static type in this paper, since the existence of the hierarchy structure and the connection of unstable manifolds are clearly demonstrated numerically for this case.

It is instructive to explain the simplest case of AHL here as in Figure 1.2 where there exist only one limiting point of a Turing branch of 2-mode. Here ‘2-mode type’ means the Fourier-mode number of the associated eigenfunc-

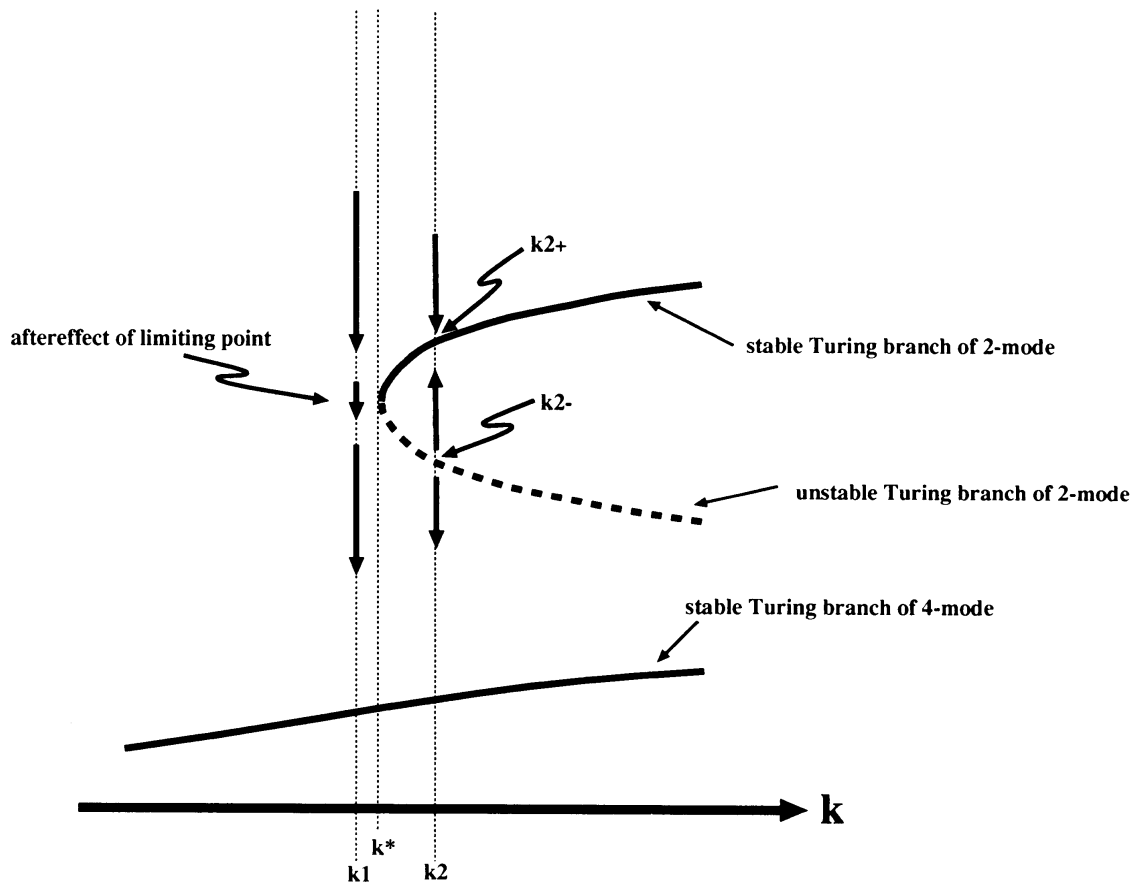


Fig. 1.2. A basic mechanism for self-replication of static type.

tion at the bifurcation point. Suppose one takes a parameter value at  $k = k_1$  which is right after the saddle-node bifurcation where a Turing branch of 2-mode already disappear there, and starts with an initial data of pulse shape which is close to a stable 2-mode Turing pattern at  $k = k_2$  near the limiting point. The pulse behaves like stationary solution for a while, and then jumps to a Turing branch of 4-mode (Figure 1.3). The replication occurs exactly when the orbit leaves the area close to the limiting point in the phase space. At  $k = k_2$ , there are three stationary solutions in Figure 1.2. The unstable 2-mode Turing pattern ' $k_2-$ ' has one unstable eigenvalue and the associated unstable manifold is connected to the stable Turing branch of 4-mode. At  $k = k_1$  the Turing patterns of 2-mode disappear through the limiting point at  $k = k^*$ , however the vector field nearby change continuously, and hence the orbit is strongly influenced by the connection of stable and unstable manifold mentioned above. Namely the 2-mode pattern

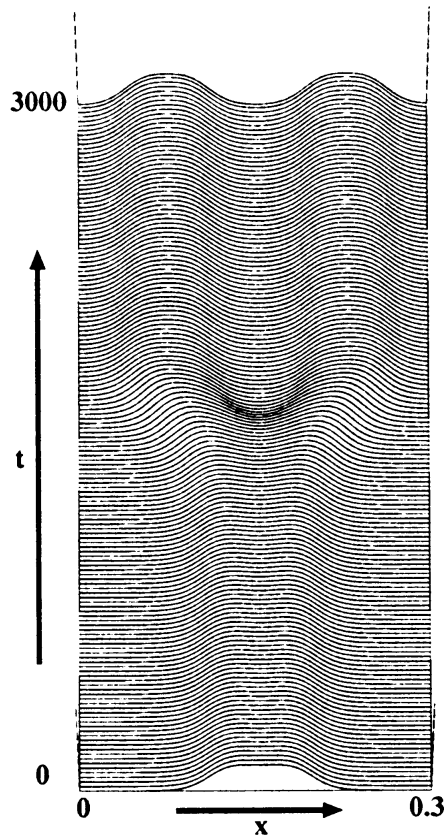


Fig. 1.3. Splitting of 1-pulse.

**must** split to 4-mode in this situation, if the initial profile is appropriately chosen. Nevertheless the magnitude of the vector field near the limiting point is very small, so the pattern stays there like a stationary pattern for a while. We call this phenomenon “aftereffect of a limiting point.” When the system size becomes larger, many limiting points line up like Figure 3.2 with similar connections above. We will show numerically that the Gray-Scott model has such a high hierarchy structure when the system size is large. We conclude therefore that the SRP is caused by AHL. The SRP of propagating type is also observed in the Gray-Scott model when the parameter  $F$  becomes smaller. We discuss about the relation between two kinds of SRP in the last section.

All bifurcation diagrams in this paper were produced by AUTO [9]. AUTO is originally designed to trace bifurcating branches of ordinary differential equations. We discretized the PDE system (1) to finite, but large-dimensional ODE system with fourth order discretization for diffusion

terms. Then we apply AUTO to this finite dimensional ODE system. The number of grid points in spatial direction is denoted by  $N$ . Applying the spatial discretization to the PDE system (1) with  $N$  grid points, we have a  $2N$  dimensional ODE system. The horizontal axis of a bifurcation diagram (see, for instance, Figure 2.4) is the bifurcation parameter  $k$  (see (3) for the meaning of  $k$ ) and the vertical axis represents a norm of the solution. We use  $l_2$ -norm, i.e. for  $u \equiv (u_1, \dots, u_N)$  we let

$$\|u\| = \left( \sum_{i=1}^N u_i^2 \right)^{\frac{1}{2}}. \quad (2)$$

## 2. The Gray-Scott model

The chemical reaction  $U + 2V \rightarrow 3V$  and  $V \rightarrow P$  in a gel reactor can be described by the following Gray-Scott model:

$$\begin{cases} \frac{\partial u}{\partial t} = D_u \nabla^2 u - uv^2 + F(1 - u) \\ \frac{\partial v}{\partial t} = D_v \nabla^2 v + uv^2 - (F + k)v, \end{cases} \quad (3)$$

where  $D_u$  and  $D_v$  are diffusion constant for the chemical materials  $U$  and  $V$  respectively. And  $F$  represent the supplying rate of  $U$  from outer reservoir and  $F + k$  represent the removal rate of  $V$  from reaction field, and  $P$  is an inert product.

The corresponding kinetics of the Gray-Scott model is given

$$\begin{cases} \frac{du}{dt} = -uv^2 + F(1 - u) \\ \frac{dv}{dt} = uv^2 - (F + k)v. \end{cases} \quad (4)$$

The nullclines and the typical flows are drawn in Figure 2.1. The solid curve represents the nullcline for  $u$  and the dotted curve as well as horizontal line constitutes that of  $v$ . Intersections of those nullclines are equilibrium points and they are represented by small disks. The black disk is a stable equilibrium, and white disk is an unstable one.

The trivial state  $(u, v) = (1, 0)$  always exists and is stable for all  $k$  and  $F$ . The phase diagram with respect to  $(k, F)$  is drawn in Figure 2.2. When  $k$  is large, the system is mono-stable (Figure 2.1 ①). All orbits approach

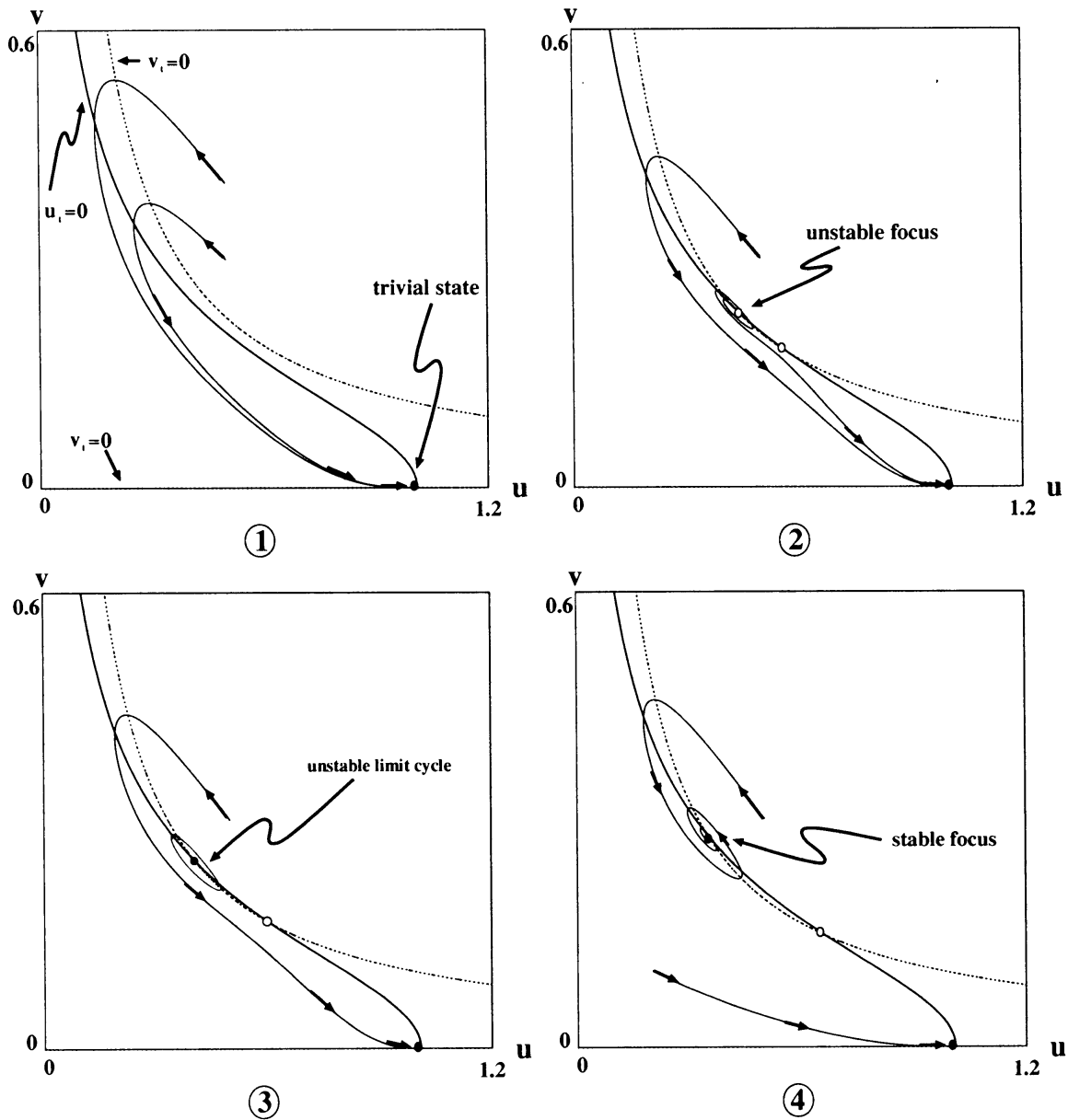


Fig. 2.1. The dynamics near the BT point.

the trivial state  $(1, 0)$ . The solid (resp. dotted) curve in Figure 2.2 shows saddle-node (resp. Hopf) bifurcation points. These two curves collide each other at  $(k_c, F_c) = (\frac{1}{16}, \frac{1}{16})$ , which is a codimension 2 point called Bogdanov-Takens type. Inside the region bounded by the solid line, there are three equilibrium points. Above the dotted line and below the upper solid line, the system is bi-stable.

Most interesting case occurs when  $F$  is smaller than  $F_c$ . When  $k$  decreases for a fixed  $F (< F_c)$ , two unstable equilibria appears via saddle-node

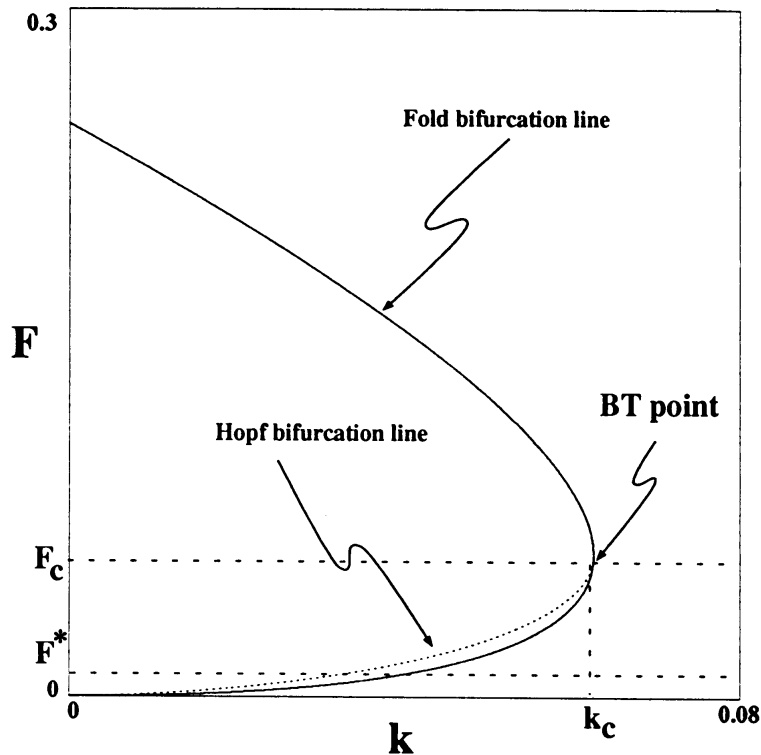


Fig. 2.2. A phase diagram of kinetics of Gray-Scott model (4).

bifurcation, then one of them changes from an unstable node to unstable focus (Figure 2.1 ②), and eventually recovers its stability via Hopf bifurcation. The Hopf bifurcation is of subcritical (resp. supercritical) type when  $F >$  (resp.  $<$ )  $F^* \approx 0.0116$  and the resulting periodic orbits are unstable (Figure. 2.1 ③). For  $F > F^*$ , the unstable periodic solution becomes larger and larger when  $k$  decreases, and becomes a homoclinic orbit to the saddle point at  $k = k_{homo}$  (see the curve 'P' in Figure 2.3), then disappears after that (Figure 2.1 ④).

A magnified phase diagram around the BT bifurcation point is Figure 2.3. Dotted curve denoted as 'H' represents Hopf bifurcation points and solid curve denoted as ' $L_+$ ' and ' $L_-$ ' represent saddle-node bifurcation points. The Hopf bifurcation points in this parameter range are subcritical, so the unstable limit cycle exists in ③ region. The curve denoted as 'P' represents saddle-homoclinic bifurcation points. The bifurcation diagram at  $F = 0.04$  with respect to  $k$  is depicted Figure 2.4. The filled square represents a Hopf bifurcation point and white circles represent the unstable periodic solutions and ' $L_-$ ' represents a saddle-node bifurcation point and 'P' represents a saddle-homoclinic bifurcation respectively.

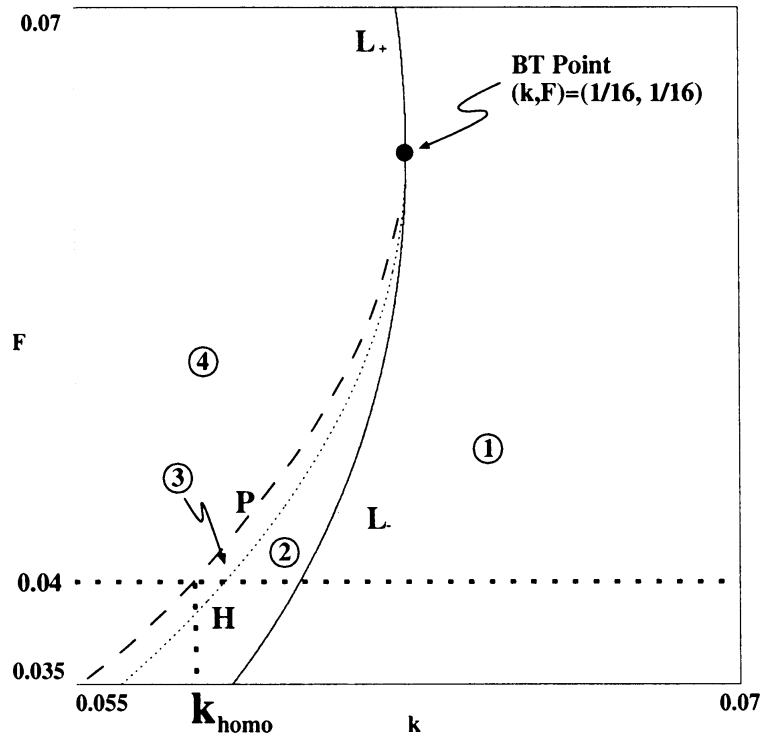


Fig. 2.3. A phase diagram near the Bogdanov-Takens (BT) bifurcation point. The numbers correspond to the flows in Figure 2.1. The curve 'P' represents the saddle-homoclinic bifurcation points.

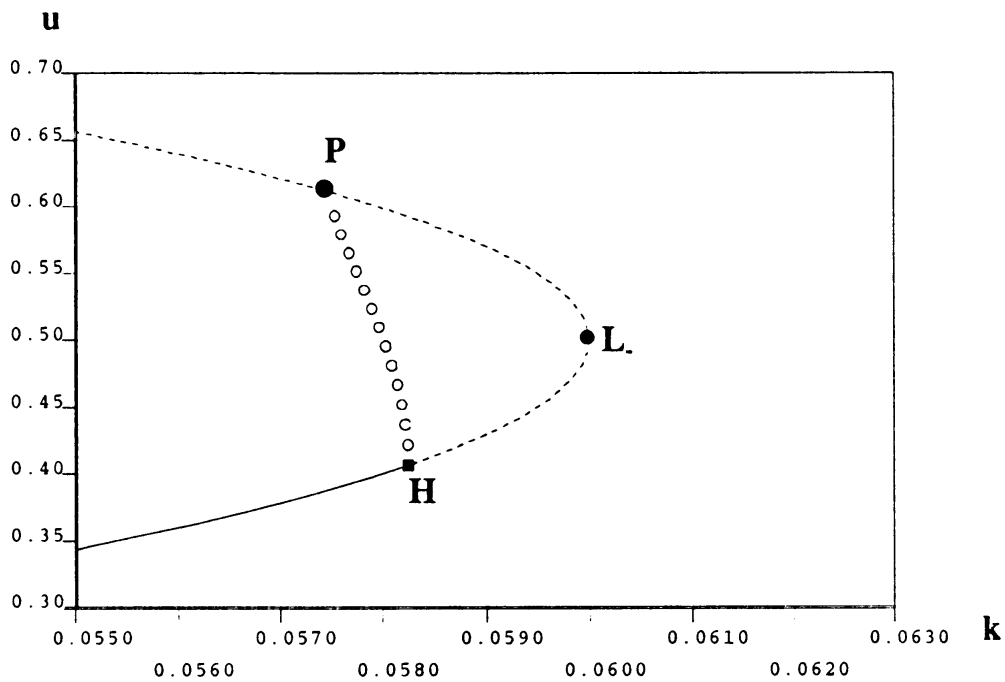


Fig. 2.4. A bifurcation diagram of ODE kinetics (4) for at  $F = 0.04$ .

### 3. Self-replicating patterns in the one dimensional Gray-Scott model

#### 3.1. Self-replicating patterns

In the previous paper [12], we presented a hidden structure for the SRP of **propagating** type with different model. The hierarchy structure of the limiting points of **oscillatory** branches (i.e., time periodic solutions of pulse type) played an important role for self-replication dynamics. In this paper, we focus on a SRP of **static** type that is caused by hierarchy structure of limiting points of **stationary** branches. The advantage of this case is that it is much more easier to trace the stationary solution branches than oscillatory ones as in [12].

The aim in this section is to show that the Gray-Scott model has the following properties:

- The limiting points of the stationary Turing branches line up at almost the same parameter value.
- The self-replicating pattern of static type occurs at the parameter value near the limiting points where stable and unstable Turing branches disappear through the saddle-node bifurcation.
- An unstable Turing pattern near the limiting point has only one unstable real eigenvalue and the associated unstable manifold of lower mode is connected to the stable Turing pattern of higher mode.

The third one is quite important in the sense that such a connection between a lower mode Turing branch and a higher mode constitutes the backbone of the self-replication phenomenon, that is, if the connection does not exist, the self-replication **never** occurs. In the next subsection, we will see the details of the hierarchy structure and how it causes the SRP of static type.

#### 3.2. Self-replication of static type

Various patterns were observed by direct numerical simulations of the Gray-Scott model (3) in the 2 dimensional domain where the diffusive parameters  $D_u$  and  $D_v$  are chosen as  $D_u = 2 \times 10^{-5}$  and  $D_v = 10^{-5}$  with periodic boundary conditions [1]. In this paper, we study (3) on a finite interval under Neumann boundary conditions with the same diffusive parameters as  $D_u = 2 \times 10^{-5}$  and  $D_v = 10^{-5}$ . Also we specify the value of  $F$  as  $F = 0.04$ . Then, there are two control parameters  $k$  and  $L$  where  $L$

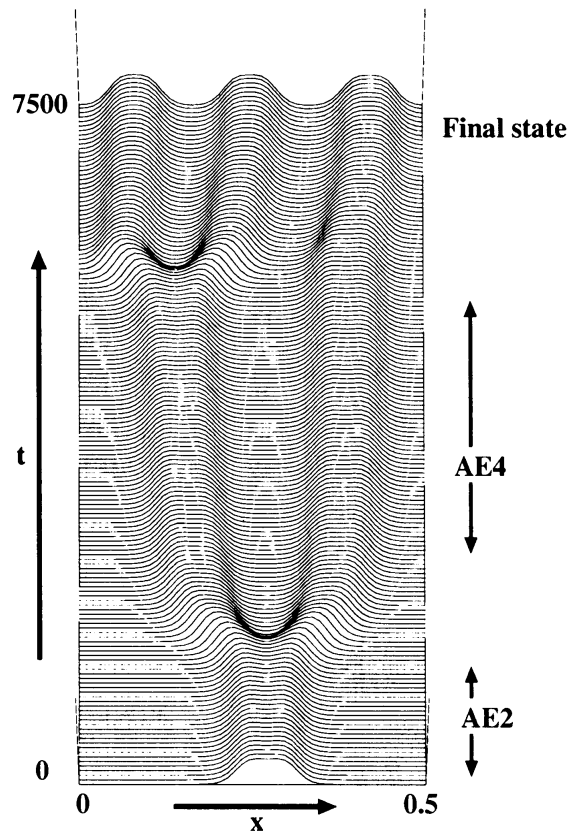


Fig. 3.1. A self-replicating pattern in the 1-dimensional Gray-Scott model ( $F = 0.04$ ,  $k = 0.06075$ ,  $L = 0.5$ ,  $N = 500$ ). The graph is a space-time plot of  $v$ .

is the system size of the PDE system, namely, it is equivalent to change the diffusivity. In this parameter setting, we can observe the 1 dimensional SRP for a suitable  $L$  and  $k$  (Figure 3.1). Under the same parameter setting, the bifurcation diagram of stationary solutions is given by Figure 3.2, which contains the information of their stabilities. The dark lines are stable stationary solutions and the light gray lines are unstable ones. We omit the labels of the bifurcation points in Figure 3.2 for simplicity. Apparently the existence of the hierarchy structure of limiting points of stationary branches is observed, which lines up near the parameter value  $k = 0.0608$ . A limiting point on the top of the diagram is a limiting point of 1-mode Turing branch. A second one is a limiting point of 2-mode Turing branch and third one is of 3-mode branch, etc. Here '1-mode type' means the Fourier-mode number of the associated eigenfunction at the bifurcation point. The value

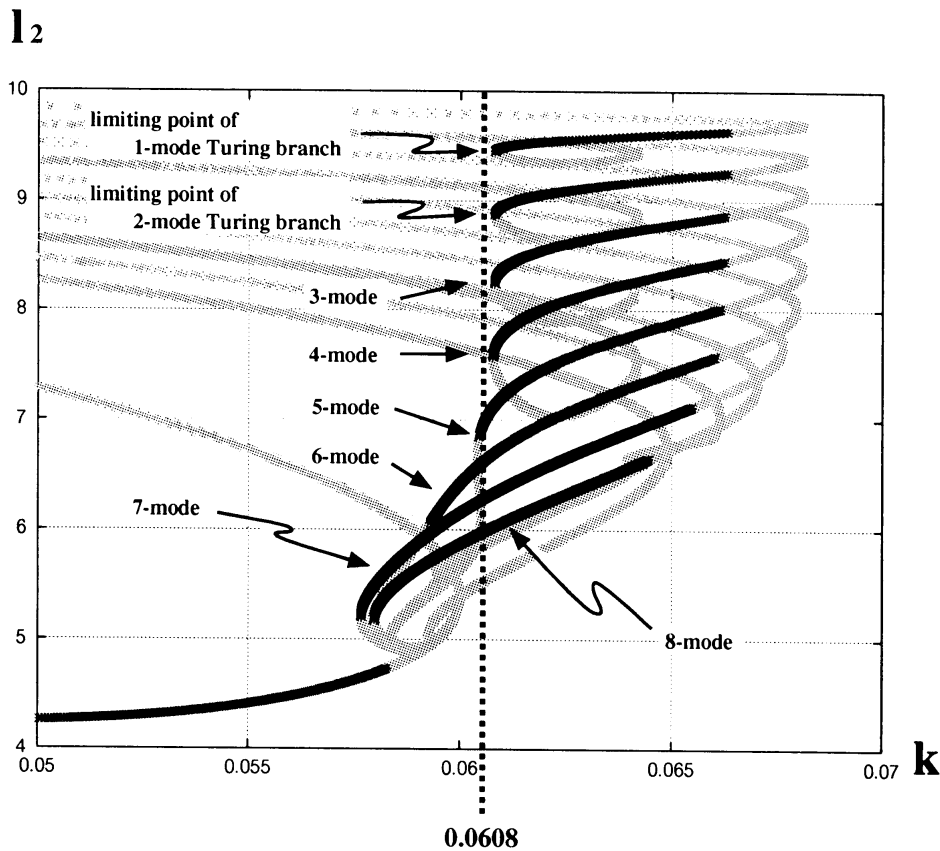


Fig. 3.2. A bifurcation diagram for  $F = 0.04$ ,  $L = 0.5$ ,  $N = 100$ .

of  $k = 0.06075$  that is used in the previous simulation (Figure 3.1) is very close to the value where the limiting points of 1,2,3 and 4-mode Turing branches line up. Notice that, there are no stable 1,2,3 and 4-mode Turing branches in the solution space at  $k = 0.06075$ . For simplicity, we present a schematic bifurcation diagram Figure 3.3. Suppose one take a parameter value at  $k = 0.06075$  which is right after the limiting point where the 1,2,3 and 4-mode stationary solutions already disappear there, and starts with an initial data of 2-mode Turing pattern which is taken from the stable Turing branch at  $k = 0.0609$  near the limiting point. It behave like a 2-mode stationary pattern for a while, and then jumps (splits) to a 4-mode pattern. The 4-mode pattern also behave like a stationary pattern for a while, and then jumps (splits) to a 6-mode pattern. The 6-mode Turing branch lies bottom of the diagram and it is stable at this value of  $k$ .

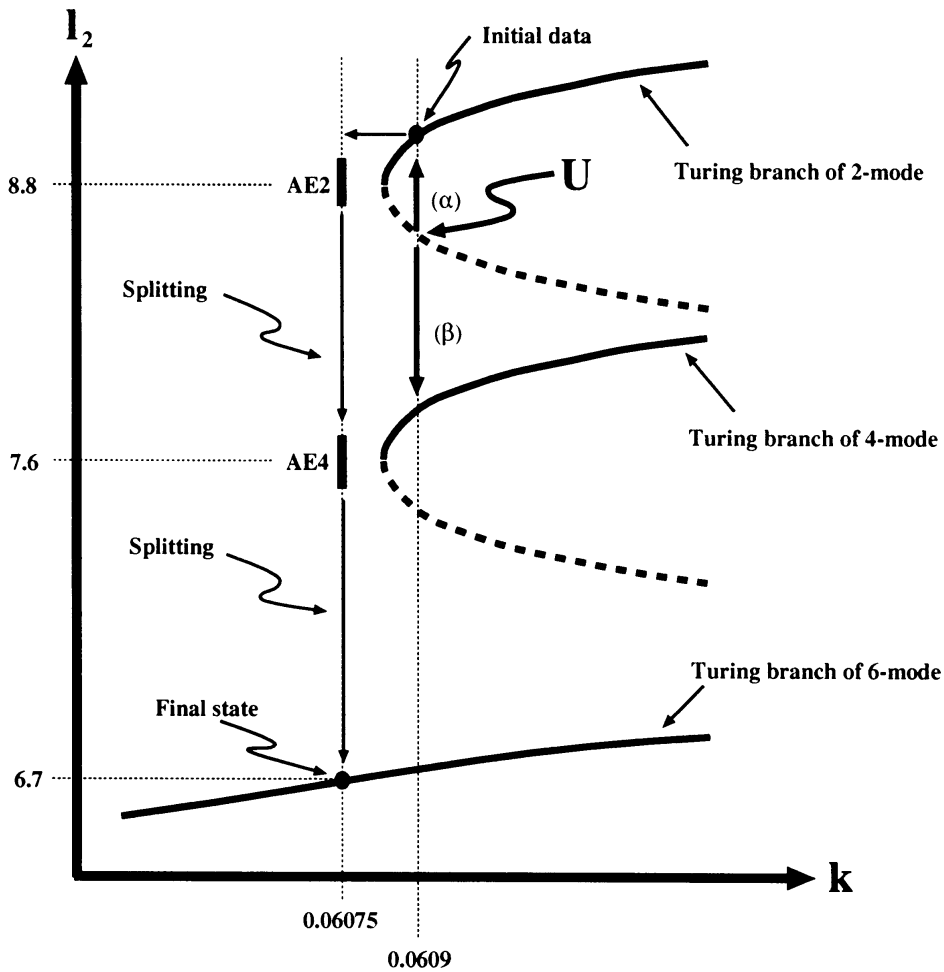


Fig. 3.3. A schematic bifurcation diagram at  $L = 0.5$ . Only the 2, 4 and 6-mode Turing branches are drawn here.

The different expression of this simulation result gives us a clear explanation of the fact (Figure 3.4). The value of the norm where the first plateau region denoted as AE2, namely the aftereffect of the limiting point of the 2-mode Turing branch, is about 8.8. This value coincides the value of the limiting point of the 2-mode Turing branch in Figure 3.2 (see also Figure 3.3). The value of the norm where the second plateau region, namely the aftereffect of the limiting point of the 4-mode Turing branch denoted as AE4, is about 7.6. This value also coincides the value where the limiting point of the 4-mode Turing branch exists. The norm value at  $t = 7500$  is 6.7, which perfectly coincides the value of the intersection point of the stable 6-mode Turing branch at  $k = 0.06075$  in Figure 3.2.

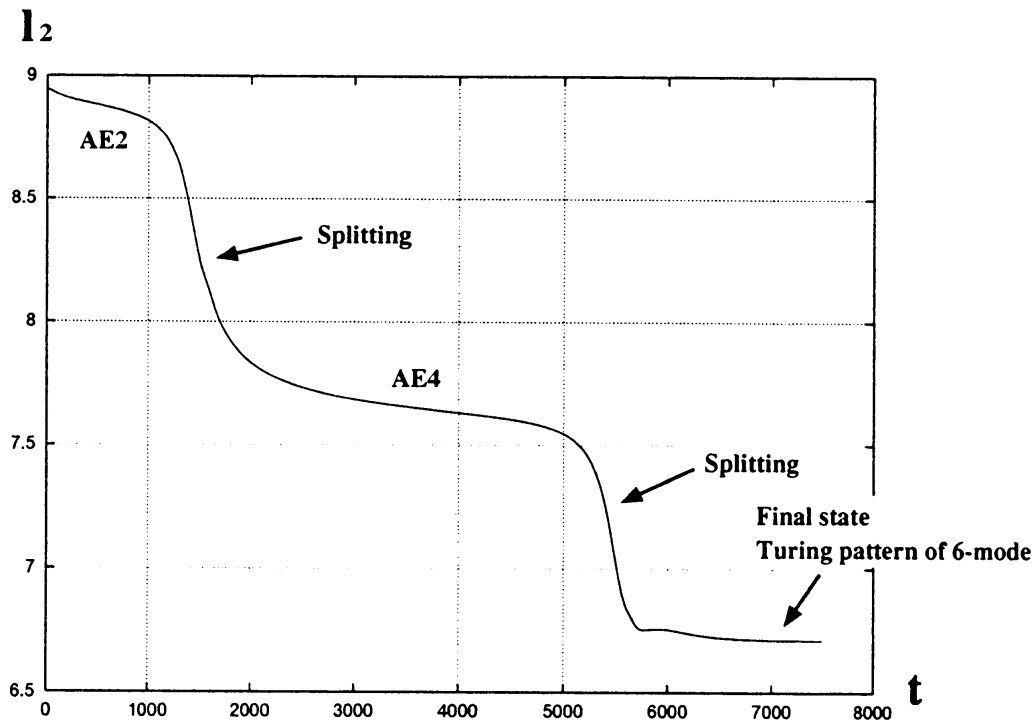


Fig. 3.4. Time-plot of the  $l_2$ -norm of the self-replicating orbit of Figure 3.1. A vertical axis is a scaled  $l_2$  norm.

The backbone structure for the SRP is the unstable manifold connecting the lower mode Turing branch to the higher mode one. The unstable Turing pattern at 'U' in Figure 3.3 has the form like Figure 3.5 (a). It has one unstable eigenvalue and the associated eigenfunction has a form like Figure 3.5 (b). Namely the unstable manifold that connects to the stable 2-mode Turing pattern and the stable 4-mode Turing pattern exists there (the arrows denoted as  $(\alpha)$  and  $(\beta)$  in Figure 3.3). To confirm the existence of such unstable manifold, we make a simulation experiment like Figure 3.6. Along this unstable manifold in the direction of  $(\beta)$ , the 2-mode pattern **must** split to the 4-mode pattern. Namely the aftereffect of the limiting point is the aftereffect of the unstable manifold that have been connected to the higher mode Turing pattern before the limiting point.

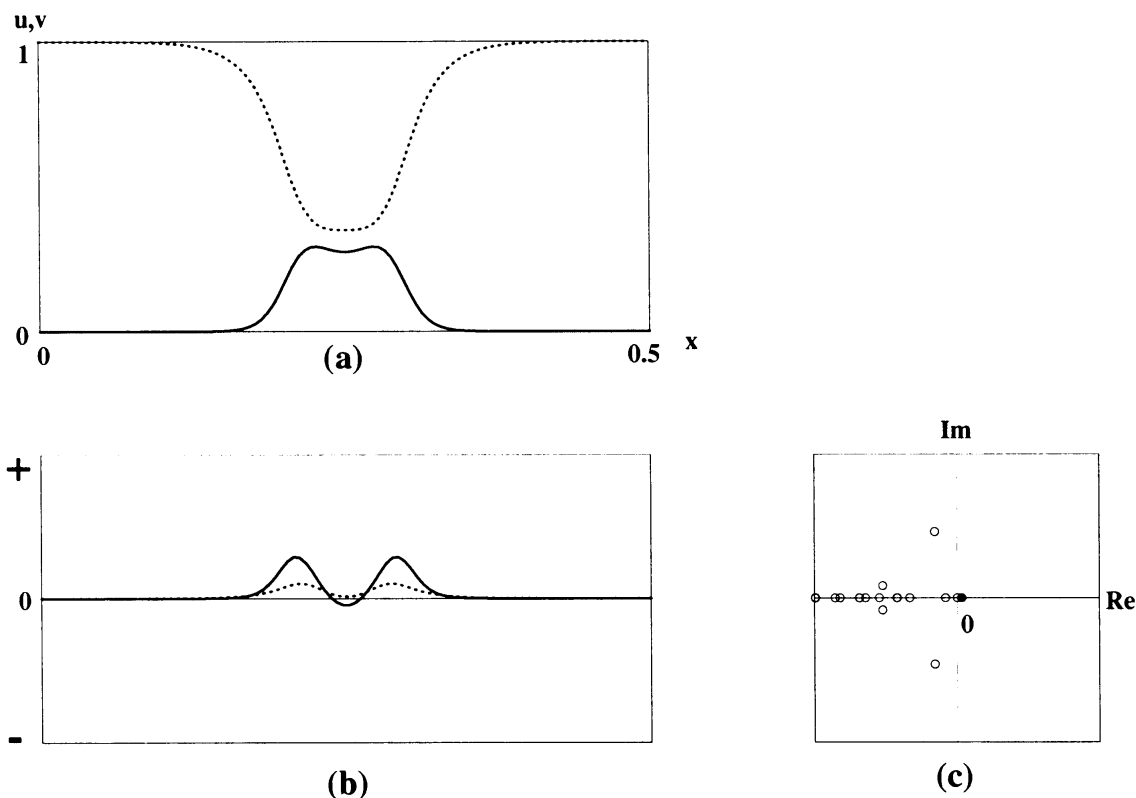


Fig. 3.5. (a): The unstable Turing pattern of 2-mode at ‘ $U$ ’ in Figure 3.3. The dotted line represents the profile of  $u$  and the solid line represents that of  $v$  respectively.  
 (b): The form of the unstable eigenfunction corresponds to the unstable eigenvalue (black filled disk) in (c).  
 (c): The distribution of the eigenvalues. There is only one unstable eigenvalue represented by black disk.

Note that if we choose the value of  $k$  smaller than previous one, namely a little bit far away from limiting point, the aftereffect of the limiting points becomes weak. Then, the 2-mode pattern split faster than before (Figure 3.7). Also note that the stable 6-mode Turing pattern and the stable 8-mode Turing pattern coexist at both parameter settings (see Figure 3.2),

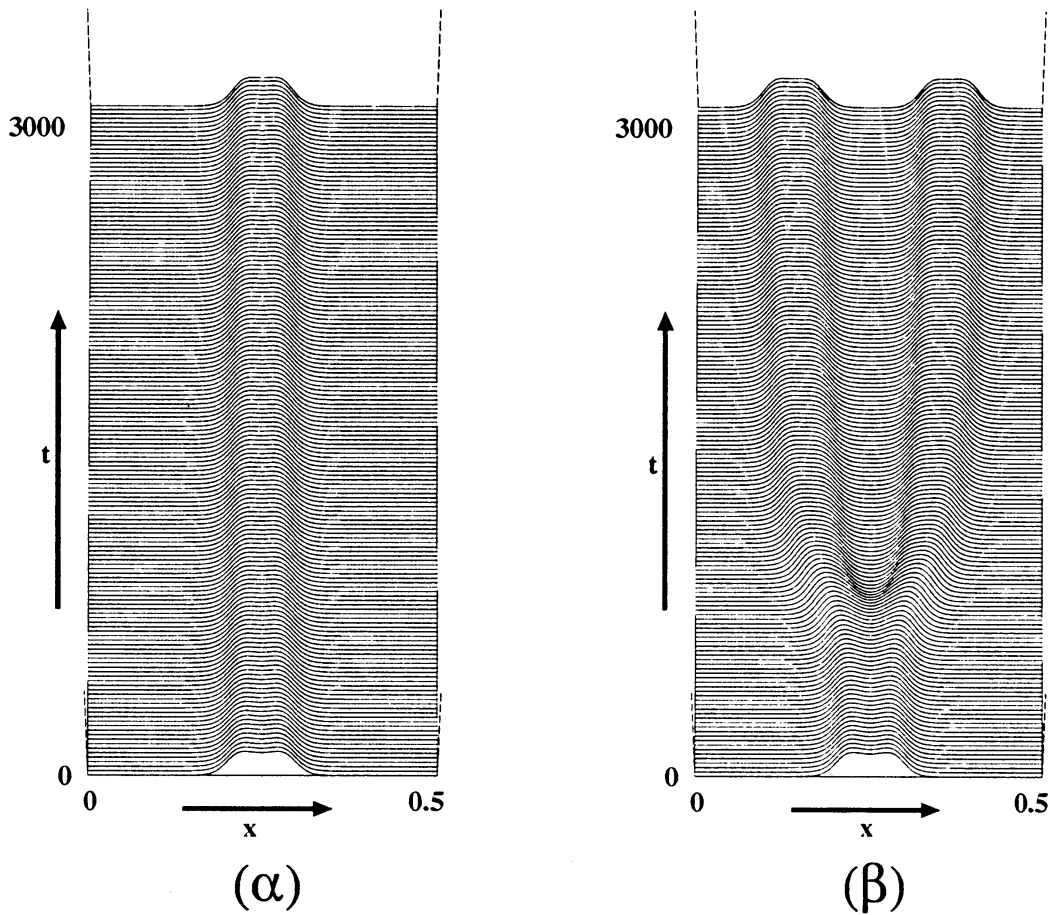


Fig. 3.6. A simulation starting from the perturbed unstable 2-mode Turing pattern of Figure 3.5 (a) ( $F = 0.04$ ,  $k = 0.0609$ ,  $L = 0.5$ ,  $N = 100$ ).

( $\alpha$ ): An addition of small negative multiple of unstable eigenform (Figure 3.5 (b)) to this unstable Turing pattern leads to the stable 2-mode Turing pattern.

( $\beta$ ): The positive perturbation leads to the stable 4-mode Turing pattern. (see also Figure 3.3)

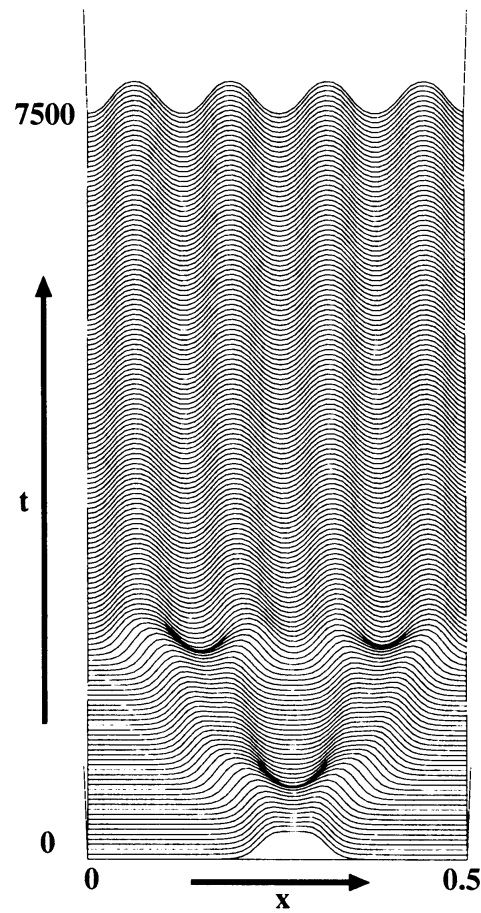


Fig. 3.7. A self-replicating pattern in the 1-dimensional Gray-Scott model ( $F = 0.04$ ,  $k = 0.0605$ ,  $L = 0.5$ ,  $N = 500$ ).

therefore the slight difference of the initial data causes the different final state generally. In fact, the final state was 6-mode Turing pattern in former case and in latter case the orbit settles down to the 8-mode Turing pattern.

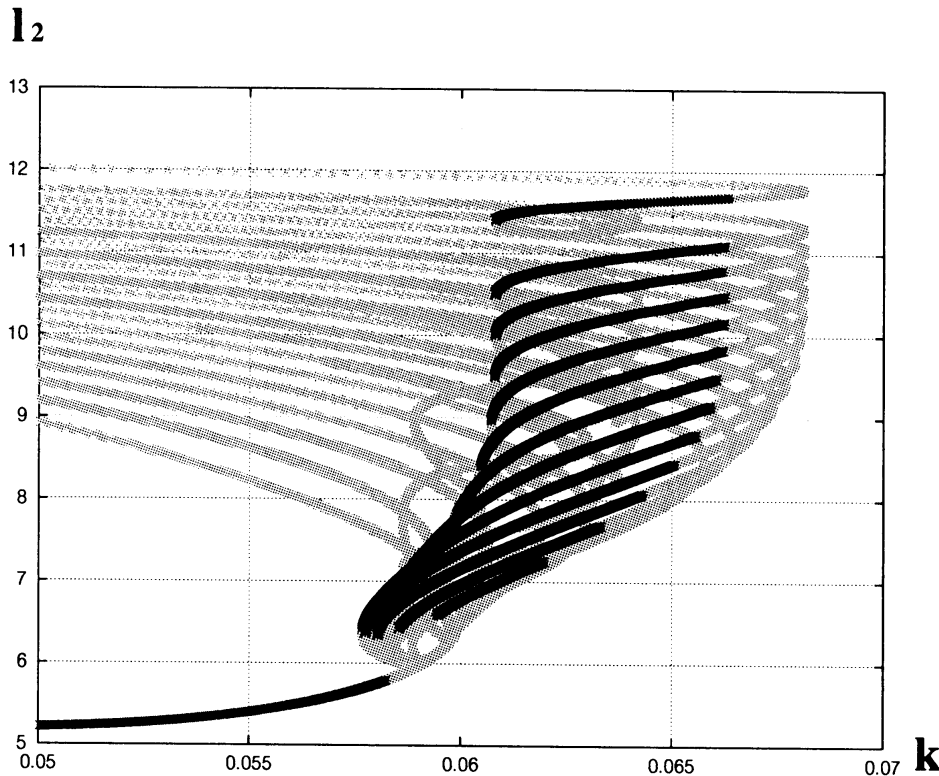


Fig. 3.8. A bifurcation diagram for  $F = 0.04$ ,  $L = 0.8$ ,  $N = 150$ .

It is easy to imagine that the hierarchy structure becomes deeper with the increase of the system size, and the duration of SRP process becomes longer. In fact, the bifurcation diagram for  $L = 0.8$  is more complicated than the previous one, but the hierarchy structure of the limiting points becomes clear and deeper than before (Figure 3.8). The orbit starting from the 2-mode pattern feels the aftereffect of the limiting point of the 2-mode branch for a while, and jumps (splits) to nearby the limiting point of the 4-mode branch. Finally, it touches down on the stable 8-mode Turing branch (Figure 3.8 and 3.9). The detailed mechanism how the limiting points are piled up will be discussed in the next section.

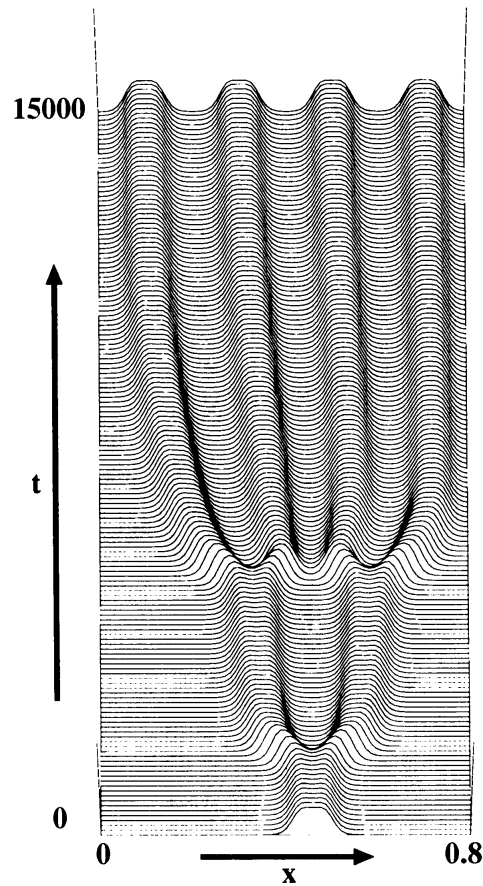


Fig. 3.9. A self-replicating pattern in the 1-dimensional Gray-Scott model ( $F = 0.04$ ,  $k = 0.06075$ ,  $L = 0.8$ ,  $N = 750$ ).

#### 4. The origin of a hierarchy structure of limiting points

In this section, we discuss about the origin of a hierarchy structure of limiting points that causes the SRP dynamics. It turns out that global bifurcational view point is quite useful to see how such a structure is formed.

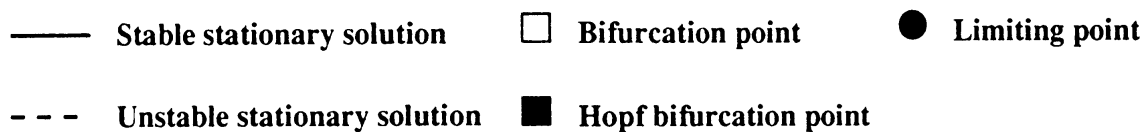


Fig. 4.1. Notation for bifurcation diagrams.

We draw the bifurcation diagrams with respect to the parameter  $k$  v.s. solution space for a given  $L$ , and see how they deform when  $L$  increases. The notation in the bifurcation diagrams is as follows (Figure 4.1).

All the Figures 4.2~4.5 contain two bifurcation diagrams; the left one is an original bifurcation diagram produced by AUTO and the right one is a simplified schematic picture. The value of norm and the value of  $k$  are accurate on the left one. The number of unstable eigenvalues of each branch is indicated in schematic diagrams.

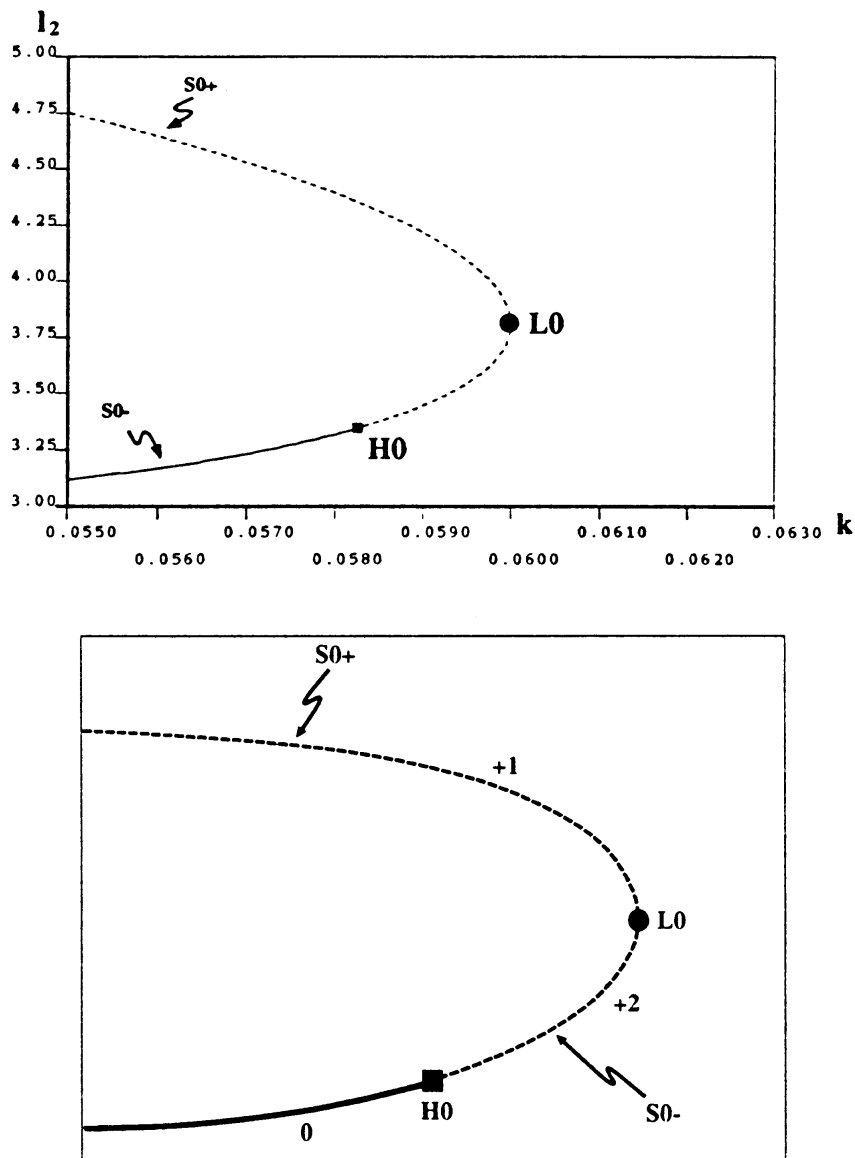


Fig. 4.2. A bifurcation diagram for  $F = 0.04$ ,  $L = 0.03$ .

### 4.1. Emergence of a limiting point of a 1-mode Turing branch

For small  $L$ , say  $L = 0.03$ , the bifurcation diagram is the same as that of the ODE kinetics (Figure 4.2). That is, there appear limiting point 'L0' of equilibria and Hopf bifurcation point 'H0' on the lower branch which ends up with a homoclinic orbit. The right figure also shows the number of unstable eigenvalues for each branches. The 'S0+' branch has one unstable eigenvalue for small  $k$  and it loses a stability through the limiting point 'L0'. Therefore, the 'S0-' branch has two unstable eigenvalues near the limiting

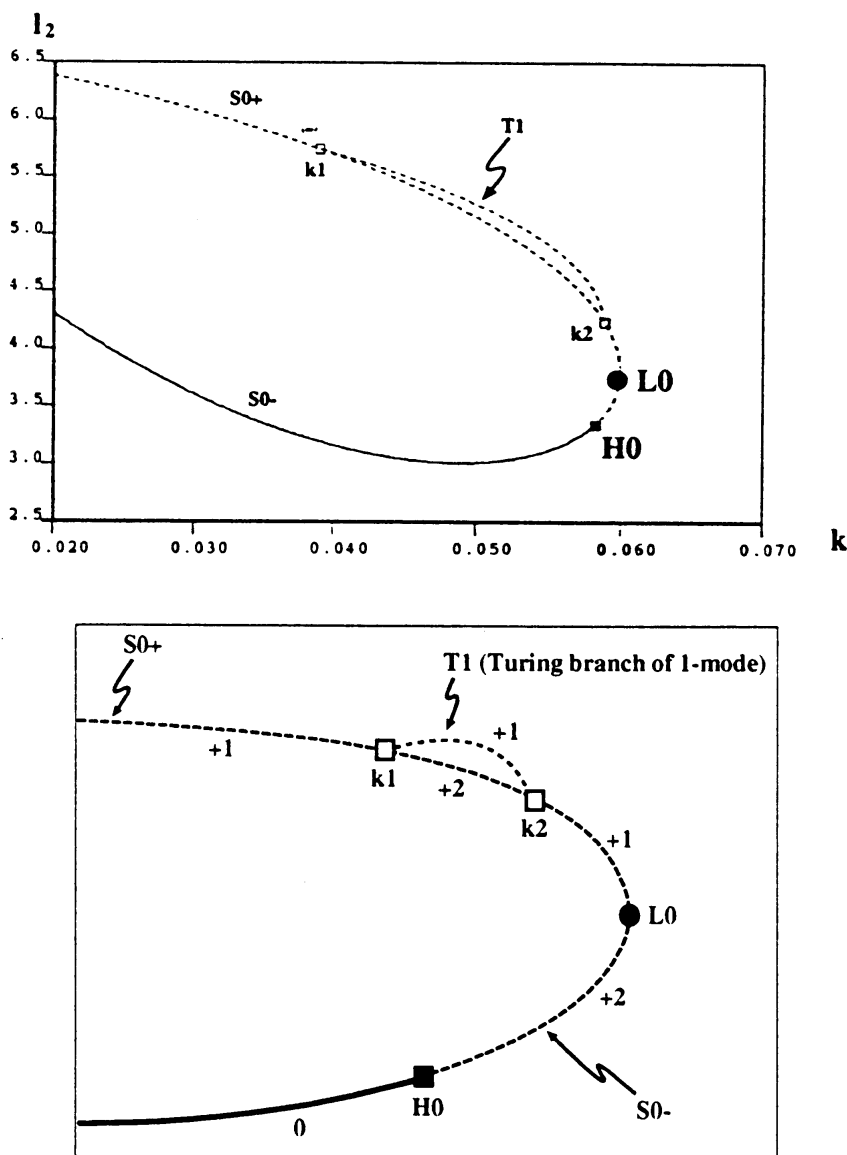


Fig. 4.3. A bifurcation diagram for  $F = 0.04$ ,  $L = 0.038$ .

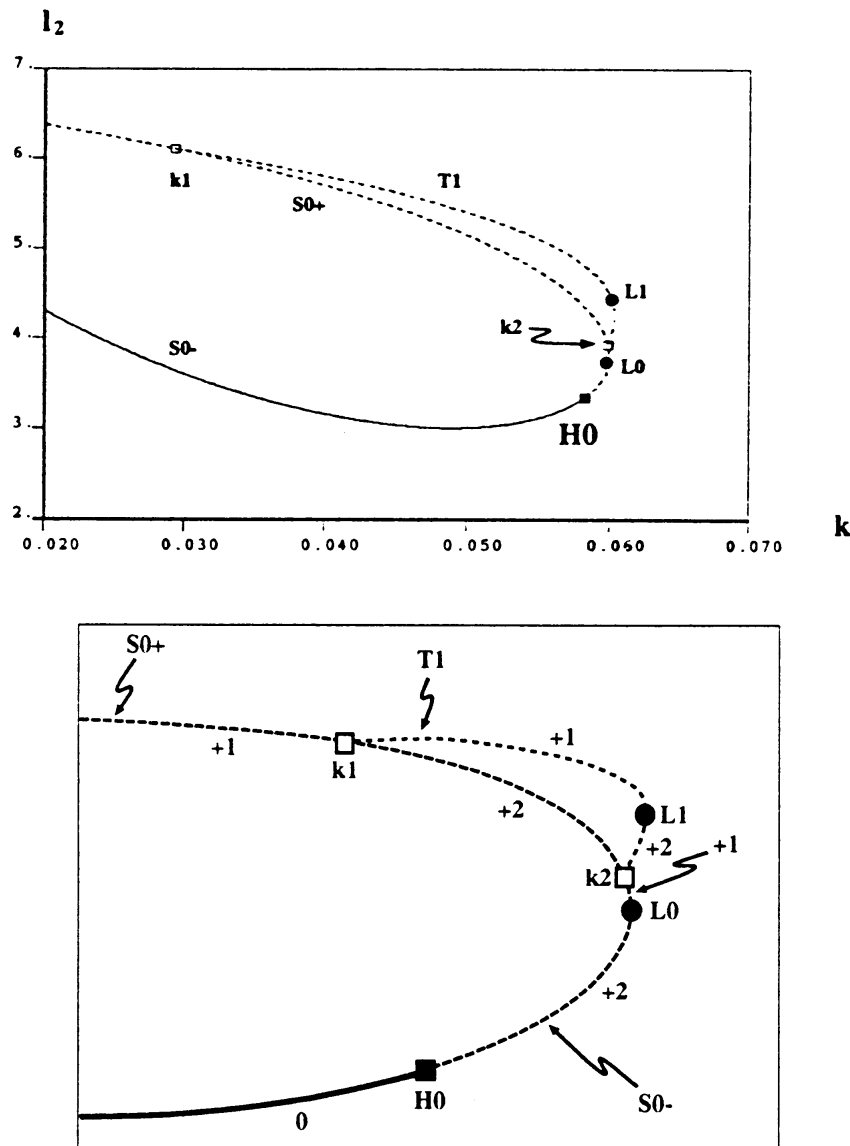


Fig. 4.4. A bifurcation diagram for  $F = 0.04$ ,  $L = 0.04$ .

point. When  $k$  decreases, the ' $S0-$ ' branch recovers its stability through the Hopf bifurcation ' $H0$ '.

When  $L$  increases, a Turing branch of 1-mode type ' $T1$ ' appears on the upper branch ' $S0+$ ' (Figure 4.3). The Turing bifurcation points are labeled as ' $k1$ ' and ' $k2$ ' respectively. At  $L = 0.038$ , ' $T1$ ' has one positive eigenvalue as in Figure 4.3, and the region on ' $S0+$ ' between ' $k1$ ' and ' $k2$ ' has two unstable eigenvalues. We are going to follow how ' $T1$ ' recovers the stability and how it will make a limiting point that forms a part of the structure for a large value of  $L$ .

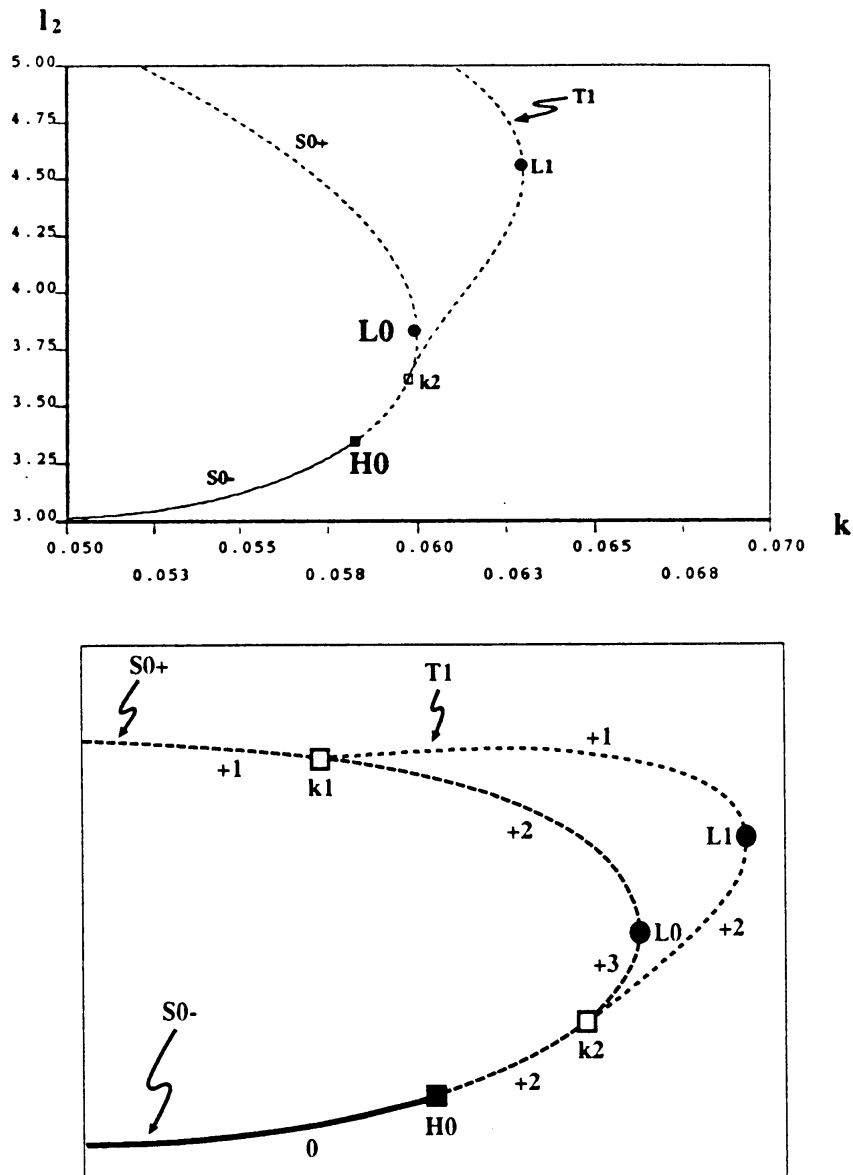


Fig. 4.5. A bifurcation diagram for  $F = 0.04$ ,  $L = 0.045$ .

When  $L$  increases, the Turing branch 'T1' overhangs and has a limiting point 'L1' on it (Figure 4.4). The region between 'L1' and 'k2' on 'T1' has two unstable eigenvalues.

At the critical value of  $L$  ( $L \approx 0.041$ ), 'k2' passes the limiting point 'L0' and it moves down to the lower branch of equilibria 'S0-' (Figure 4.5). Note that the Turing branch 'T1' overhangs the limiting point 'L0', therefore it persists over the parameter region where there are no nontrivial constant states except the trivial state  $(u, v) = (1, 0)$ , namely mono-stable region.



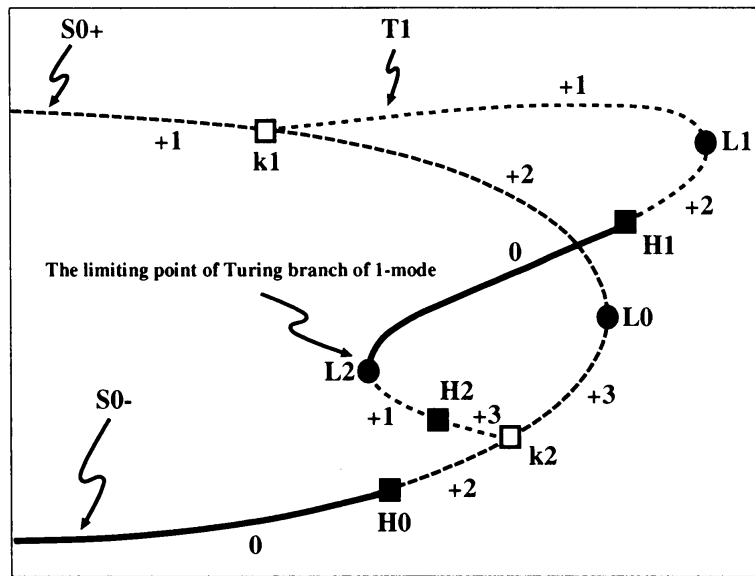


Fig. 4.8. A bifurcation diagram for  $F = 0.04$ ,  $L = 0.06$ .

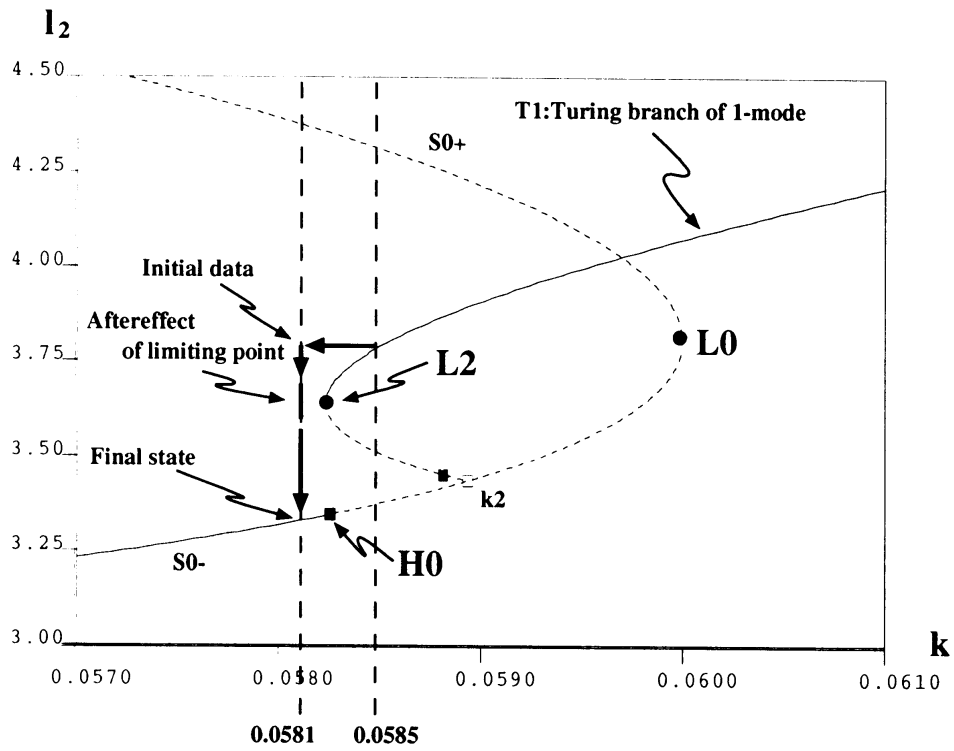


Fig. 4.9. Aftereffect of the limiting point  $L_2$  at  $F = 0.04$ ,  $L = 0.06$ .

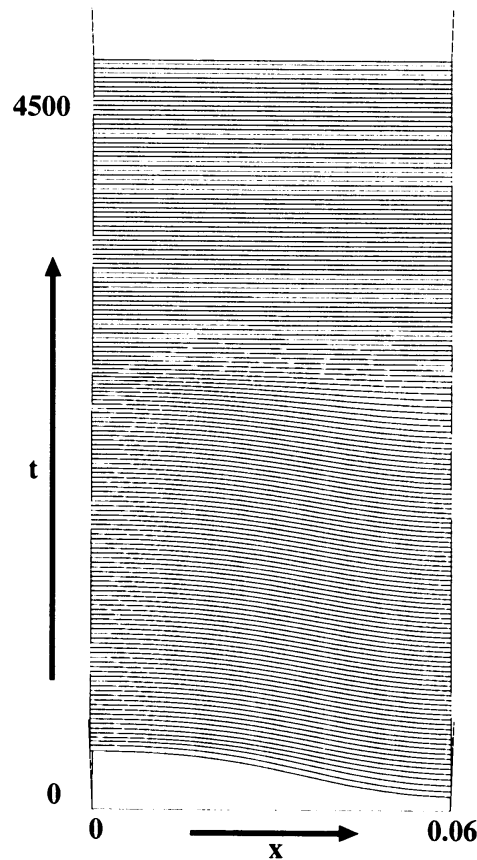


Fig. 4.10. The aftereffect of limiting point of 1-mode Turing branch ( $F = 0.04$ ,  $k = 0.0581$ ,  $L = 0.06$ ,  $N = 250$ ).

At  $L = 0.0495$ , the Turing branch ' $T1$ ' starts to deform and a new limiting point ' $L2$ ' appears on it. Therefore, ' $T1$ ' has two limiting points at this time (Figure 4.6).

At  $L = 0.05$ , a pair of Hopf bifurcation points ' $H1$ ' and ' $H2$ ' appears on ' $T1$ '. Due to the emergence of these two Hopf points, the branch between ' $H1$ ' and ' $H2$ ' gains its stability as in Figure 4.7.

For further increase of  $L$ , the Hopf bifurcation point ' $H2$ ' moves toward the limiting point ' $L2$ ' and passes it depicted in Figure 4.8. At  $L = 0.06$ , the Hopf bifurcation point ' $H2$ ' had gone over ' $L2$ ' already. As a result, one of the components of the hierarchy structure of the limiting points, namely the limiting point of the stable Turing pattern of 1-mode and the unstable Turing pattern of 1-mode is constructed.

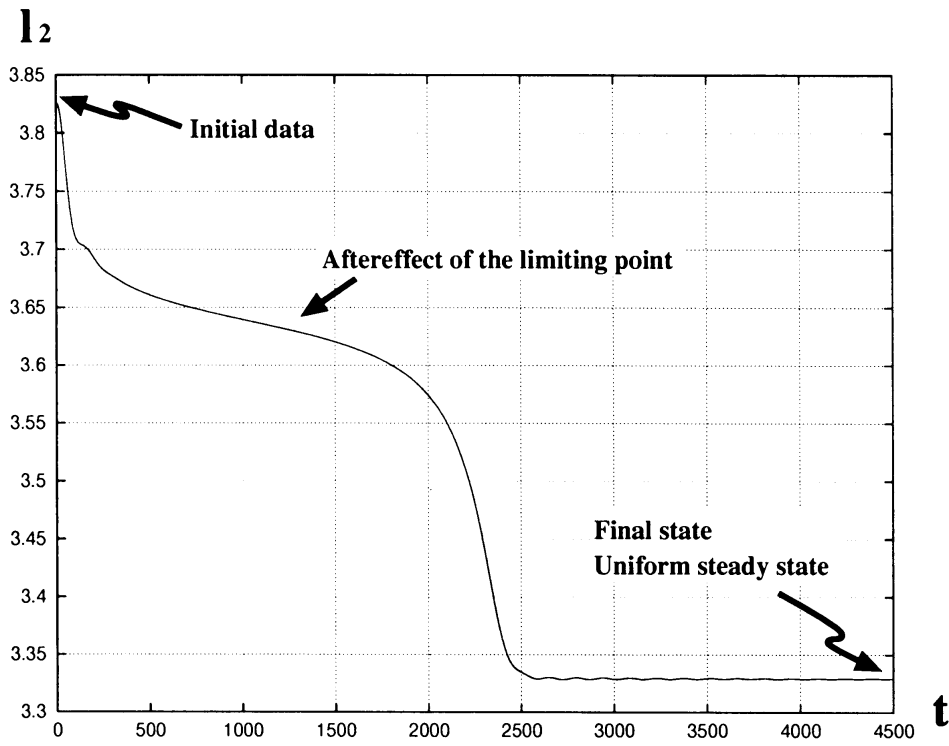


Fig. 4.11. Time-plot of the  $l_2$ -norm of the self-replicating orbit of Figure 4.10. A vertical axis is a scaled  $l_2$  norm.

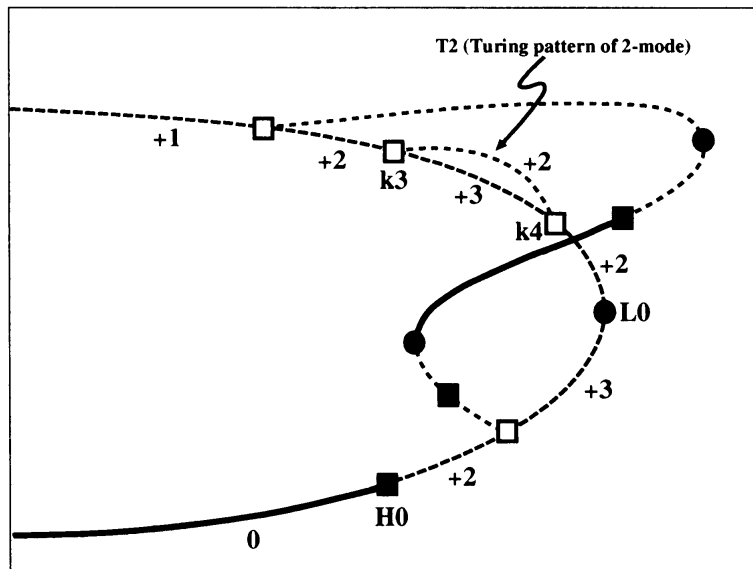


Fig. 4.12. Emergence of a Turing branch of 2-mode ( $F = 0.04$ ,  $L = 0.077$ ).

Here we check that the aftereffect of limiting point really occurs near ‘ $L2$ ’. Let  $k = 0.0581$  where all non-uniform stationary solutions already disappear there, and take 1-mode Turing pattern at  $k = 0.0585$  as a initial data (Figure 4.9). In this case, the 1-mode pattern lasts about 2000 time step, then jumps to the uniform trivial state (Figures 4.10 and 4.11).

#### 4.2. Formation of the limiting points of Turing branch of higher mode

At  $L = 0.077$ , the Turing branch of 2-mode ‘ $T2$ ’ appears (Figure 4.12). It looks similar when the Turing branch of 1-mode ‘ $T1$ ’ appears at  $L = 0.038$  before (Figure 4.3). However, the number of unstable eigenvalues is different each other, namely ‘ $T2$ ’ branch has one more unstable eigenvalue than ‘ $T1$ ’ branch. Hence ‘ $T2$ ’ branch has to recover twice to get stability. It turns out that the first recovery occurs due to the interaction between ‘ $T1$ ’ and ‘ $T2$ ’ branches.

At  $L = 0.09$ , the bifurcation point ‘ $k4$ ’ of ‘ $T2$ ’ passes the limiting point ‘ $L0$ ’ like ‘ $k2$ ’ at  $L = 0.045$  (Figures 4.5 and 4.13).

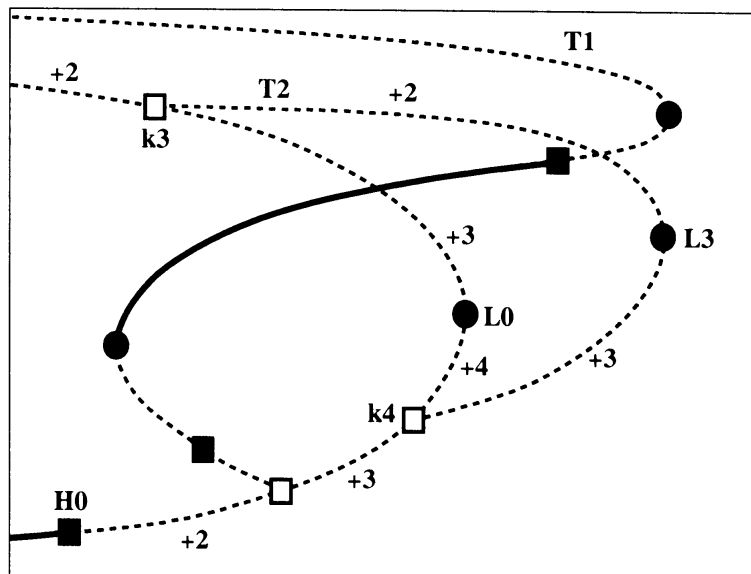
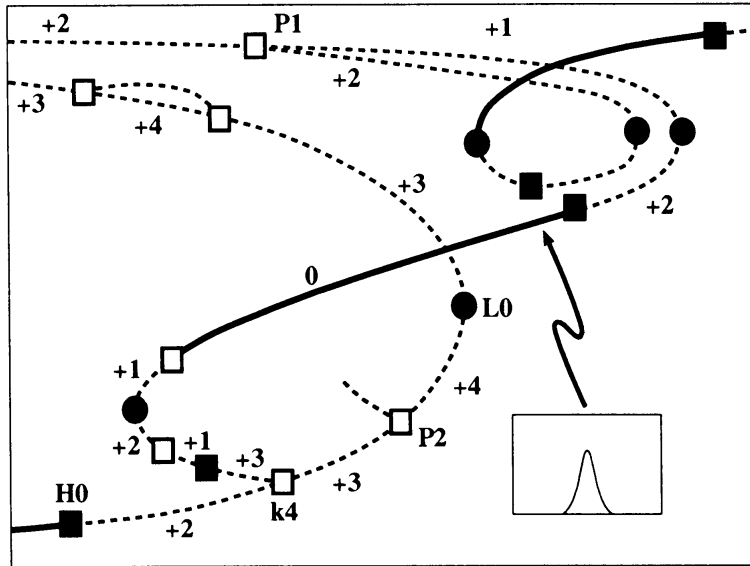
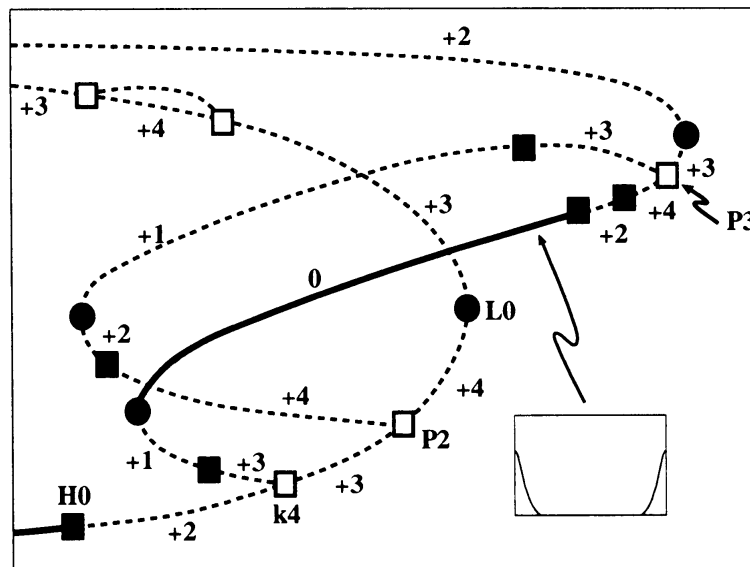


Fig. 4.13. A bifurcation diagram for  $F = 0.04$ ,  $L = 0.09$ .



(a)



(b)

Fig. 4.14. A bifurcation diagram for  $F = 0.04$ ,  $L = 0.11$ .

When  $L$  increases, the bifurcation points of 'T1' and 'T2' on 'S0-' crosses each other and start to make a rearrangement of branches. So far, we ignore the difference of a pair of solution of 'T2' depicted in Figure 4.14, which makes a loop in a solution space, although they are projected on the same branch in Figure 4.14 (recall that there are no difference in  $l_2$ -norm). However rearrangement of branches is not symmetric on these branches, in fact 'T1' is split into two parts and its upper part ends at 'P1' which is responsible for the first recovery of 'T2' branch of type (a) (see Figure 4.14 (a)). The next recovery of stability on type (a) branch occurs exactly the same way as 'T1' branch as before as in Figure 4.14 (a). On the other hand, the lower part of 'T1' branch also becomes a secondary bifurcation point at 'P3' of 'T2' of type (b) (Figure 4.14 (b)), however 'T2' loses its stability at 'P3' and the number of unstable eigenvalues becomes 4 this time. Nevertheless 'T2' recovers its stability completely by two times Hopf bifurcations as in Figure 4.14 (b).

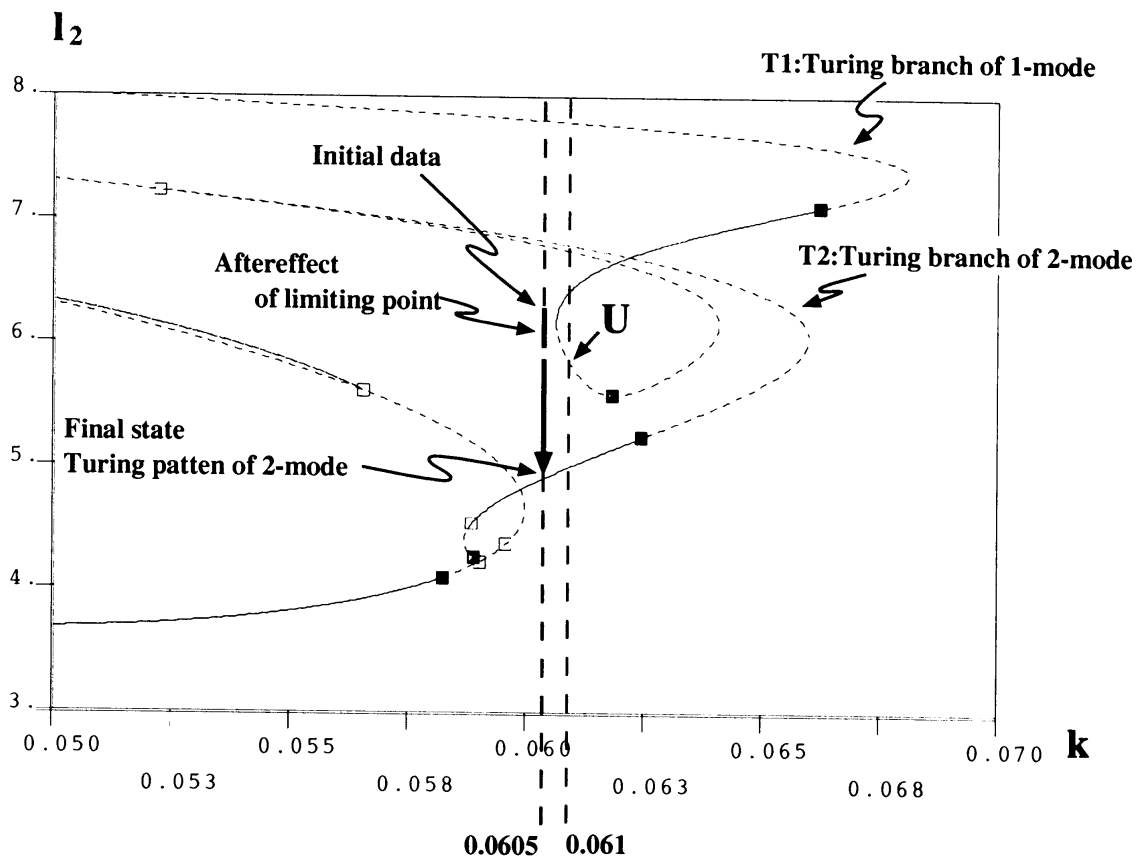


Fig. 4.15. A detailed bifurcation diagram for  $F = 0.04$ ,  $L = 0.11$ .

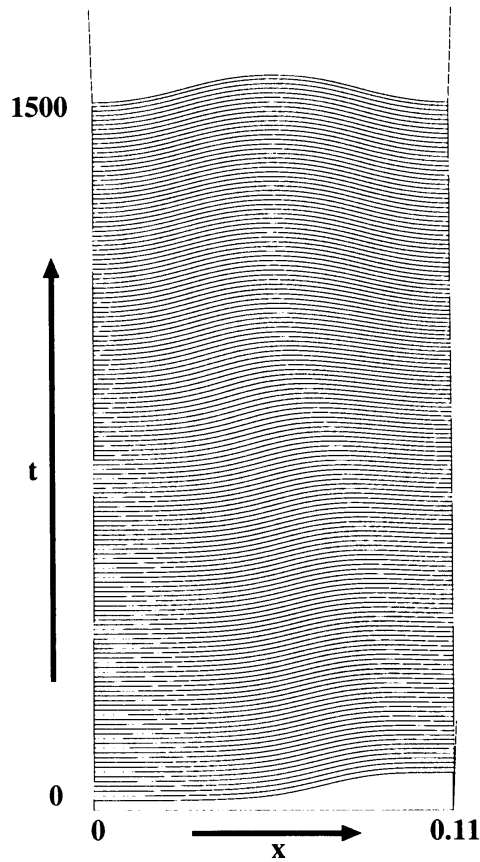


Fig. 4.16. Replication from 1-mode to 2-mode  
 $(F = 0.04, k = 0.0605, L = 0.11,$   
 $N = 375).$

The original bifurcation diagram for Figure 4.14 (a) is given by Figure 4.15. It can be observed that the splitting from 1-mode to 2-mode in this diagram. Let us take  $k = 0.0605$  and an initial data from the stable part of 'T1' at  $k = 0.061$ . The orbit behaves as in Figures 4.16 and 4.17. The unstable 1-mode Turing pattern at 'U' in Figure 4.15 has one positive eigenvalue and the corresponding eigenfunction has a form like Figure 4.18 (b). It is confirmed numerically that the associated unstable manifold of  $U$  is connected to the stable 'T2' pattern, which implies that the 1-mode pattern **must** split to the 2-mode pattern.

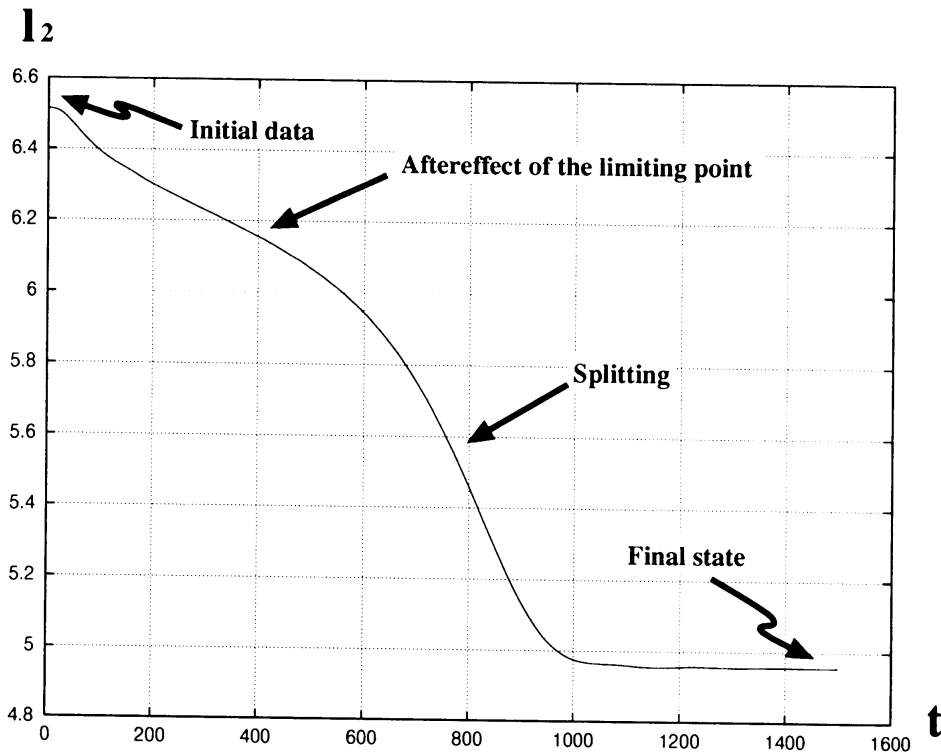


Fig. 4.17. Time-plot of the  $l_2$ -norm of the self-replicating orbit of Figure 4.16. A vertical axis is a scaled  $l_2$  norm.

When  $L$  increases, Turing patterns of higher modes recover their stabilities successively. Based on our careful dissection of the bifurcation diagram at  $L = 0.5$ , we conjecture that general even mode Turing branch, say  $2N$ -mode, is able to recover the stabilities by  $N$  times Hopf bifurcations like Figure 4.19. Nevertheless, the origin of these Hopf bifurcation points has been unknown.

## 5. Discussion

The Gray-Scott model displays a variety of dynamical patterns [1] and a phase diagram starting from an initial data of one-pulse type is given by Figure 5.1. Self-replicating patterns are observed in the region (c) which is next to the standing (resp. oscillatory) pulse region (a) (resp. (c)). It should be remarked that there are two types of SRP as in Figure 5.2: SRP of static type, which is our main concern in this paper, is typically observed near the boundary of the region (a), and SRP of oscillatory type similar to the pattern in [12] is observed near that of (b). Notice that the asymptotic

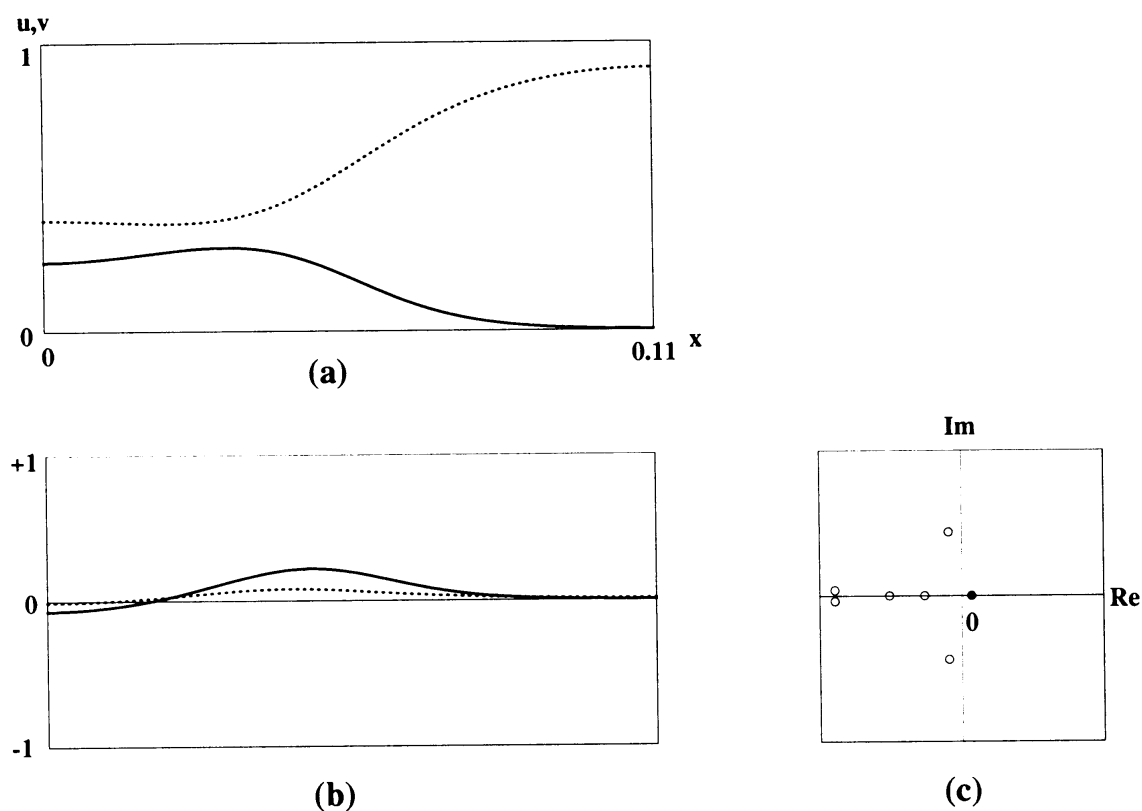


Fig. 4.18. (a): An unstable Turing pattern of 1-mode at 'U' in Figure 4.15. The dotted (resp. solid) line represents  $u$  (resp.  $v$ ).  
 (b): The form of the eigenfunction corresponds to the unstable eigenvalue corresponding to the black disk in (c).  
 (c): The distribution of the eigenvalues.

state in (c) is a stationary state if we run numerics for a long time, since SRP is a transient process from one-pulse to a steady state of Turing type. The locations of  $k$ -values ( $k = 0.06075$  and  $0.0542$ ) where the two types of SRP are observed as in Figure 5.2 are very close to the boundary of (a) (or (b)) region. This strongly suggests that the limiting points of stationary (or oscillatory) branches line up at those boundary points and there occurs an aftereffect in the region (c) as well as the disappearance of stationary (or oscillatory) branches.

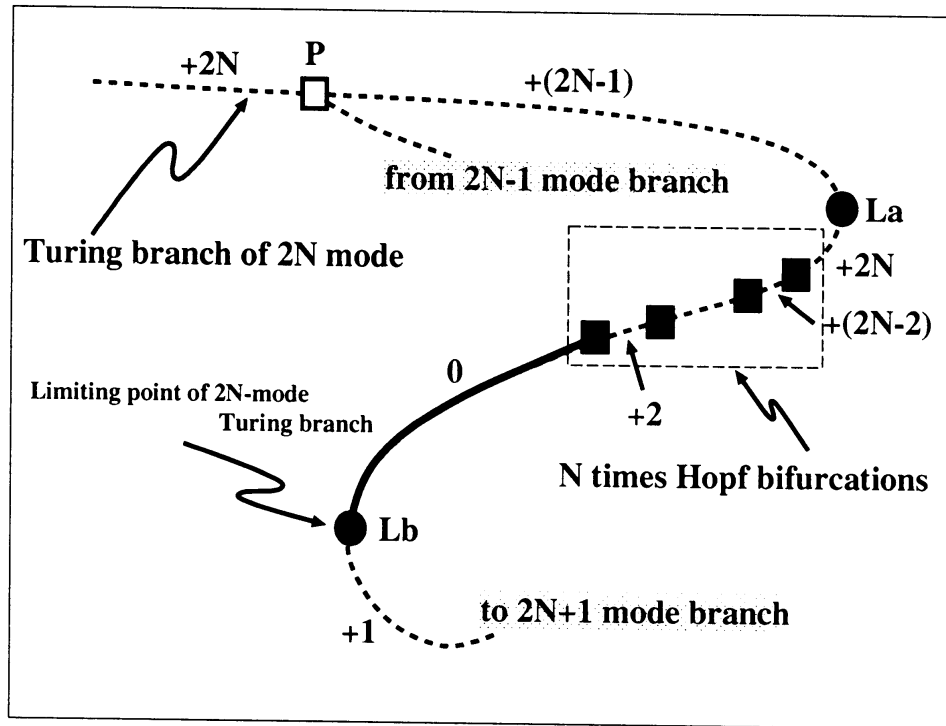


Fig. 4.19. A schematic bifurcation diagram of Turing branch of  $2N$ -mode.

The reasons why the limiting points of the stationary branches line up at almost the same value of  $k$  can be informally explained as follows. Suppose that there exists a stable 1-pulse stationary pattern with the interval  $L$ , and the value of  $k$  where the limiting point occurs is converge to the  $k^*$  with increase of  $L \rightarrow \infty$ . Because of the boundary conditions are Neumann type, there also exists a stable  $n$ -pulses stationary pattern with the interval  $nL$  and a stable 1-pulse one co-exists with the same interval. If the  $L$  is appropriately wide, the  $n$ -pulse pattern also has limiting point near the  $k = k^*$ , because one of the 1-pulse in the  $n$ -pulses sequence converges to the single 1-pulse shape with increase the interval  $L$ . Hence it is plausible that the  $n$ -pulses sequence also become unstable or ceases to exist near  $k = k^*$ .

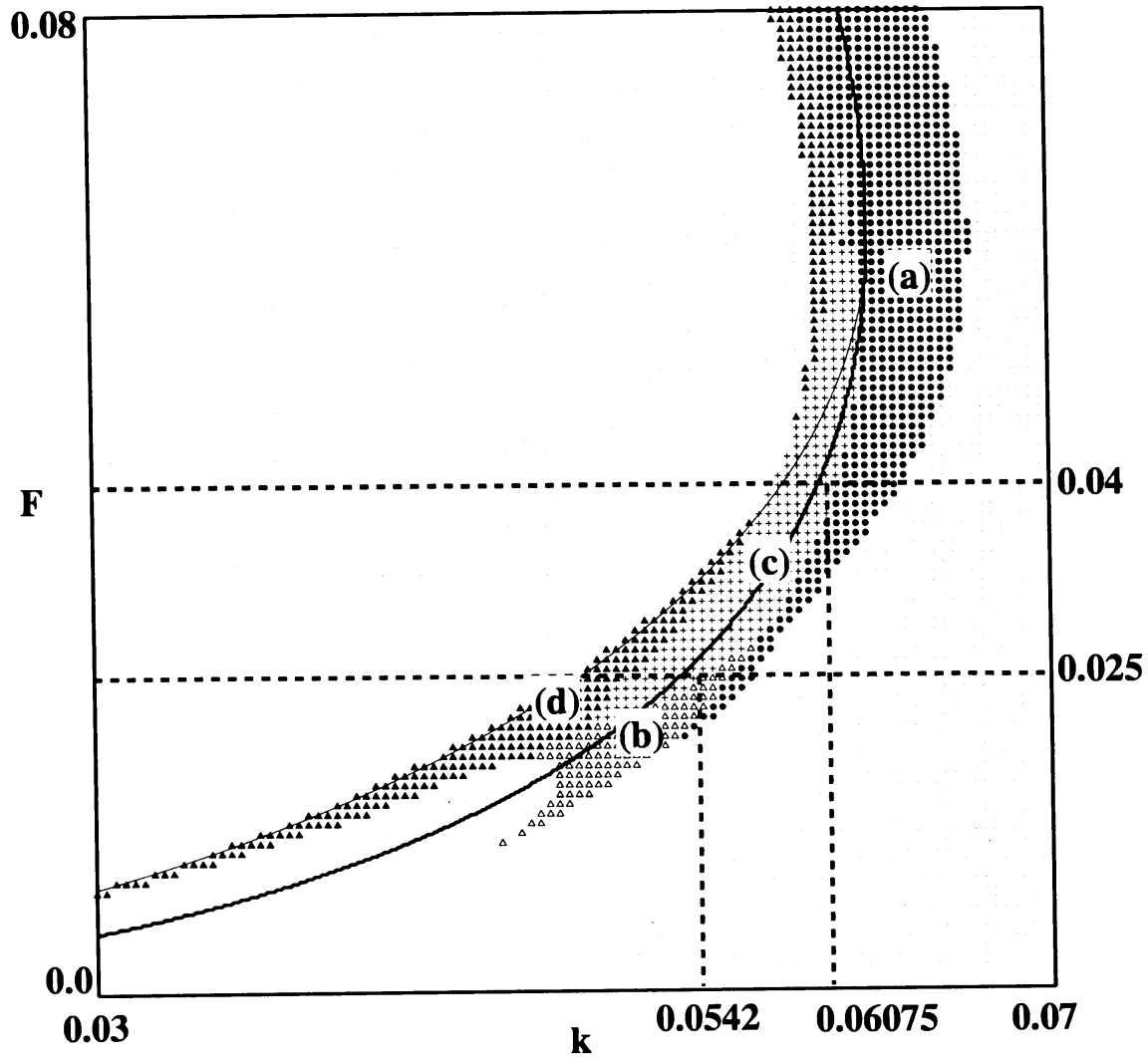


Fig. 5.1. A phase diagram of the 1 dimensional Gray-Scott model with the diffusion coefficients  $D_u = 2 \times 10^{-5}$  and  $D_v = 10^{-5}$  respectively.  
 (a): A region where stable standing pulse solution exists.  
 (b): A region where stable **oscillatory** pulse solution exists.  
 (c): A region where the SRP is observed.  
 (d): A region where the other patterns are observed those include the chaotic pattern.

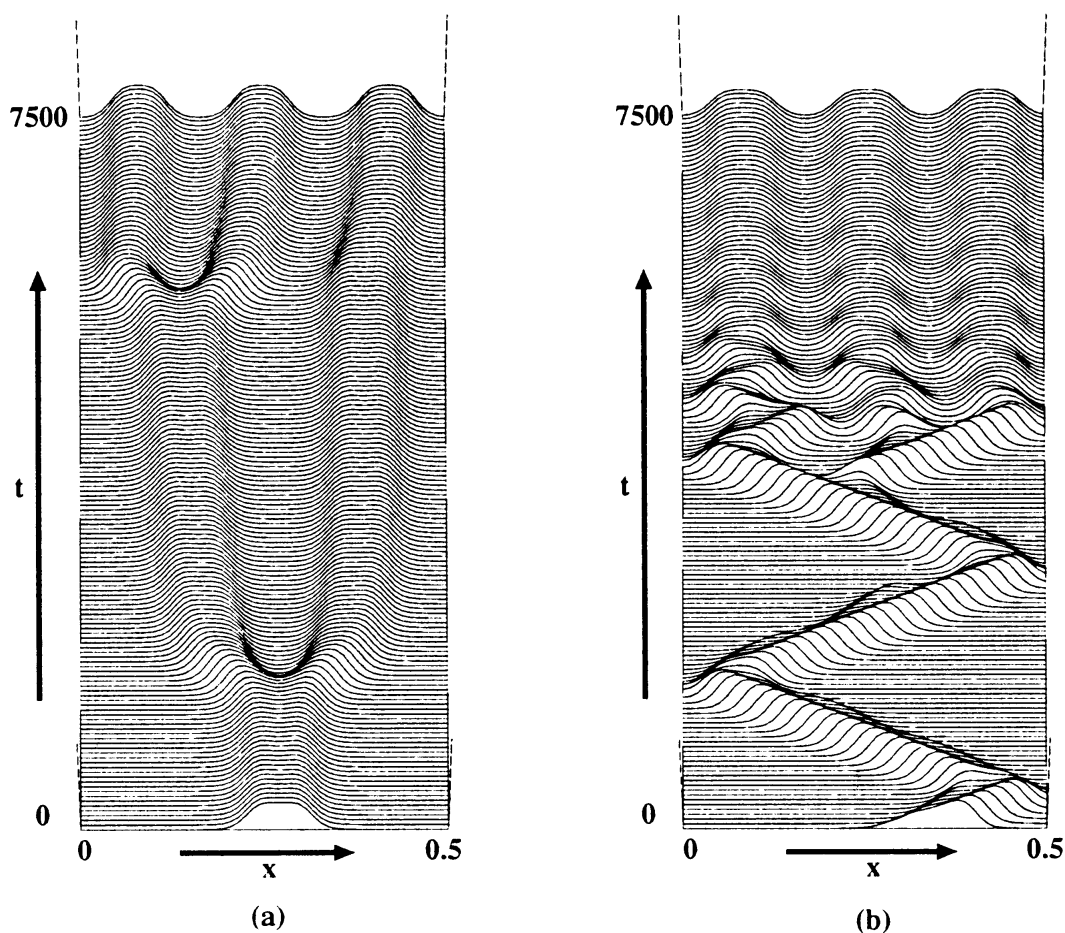


Fig. 5.2. Two types of self-replicating pattern in the 1-dimensional Gray-Scott model (3).

(a): A static type SRP at  $F = 0.04$ ,  $k = 0.06075$ .

(b): A propagating type SRP at  $F = 0.025$ ,  $k = 0.0542$ .

Both simulations were done with the diffusion coefficients  $D_u = 2 \times 10^{-5}$  and  $D_v = 10^{-5}$  respectively and the system size was 0.5. The boundary conditions were Neumann. The spatial mesh consisted of 500 grid points.

## 6. Acknowledgments

The author would like to thank Professor Yasumasa Nishiura for helpful suggestions and valuable discussions for this study.

## References

- [ 1 ] Pearson J.E., *Complex patterns in a simple system*. Science **216** (1993), 189–192.
- [ 2 ] Reynolds W.N., Pearson J.E. and Ponce-Dawson S., *Dynamics of self-replicating patterns in reaction diffusion systems*. Physical Review Letters **72**, No.17 (1994), 1120–1123.
- [ 3 ] Kepper P.De , Perraud J.J., Rudovics B. and Dulos E., *Experimental study of stationary turing patterns and their interaction with traveling waves in a chemical system*. International Journal of Bifurcation and Chaos **4**, No.5 (1994), 1215–1231.
- [ 4 ] Rasmussen K.E., Mazin W., Mosekilde E., Dewel G. and Borckmans P., *Wave-splitting in the bistable Gray-Scott model*. International Journal of Bifurcation and Chaos **6**, No.6 (1996), 1077–1092.
- [ 5 ] Petrov V., Scott S.K. and Showalter K., *Excitability, wave reflection, and wave splitting in a cubic autocatalysis reaction-diffusion system*. Phil. Trans. Roy. Soc. Lond. A **347** (1994), 631–642.
- [ 6 ] Doelman A., Kaper T.J. and Zegeling P.A., *Pattern formation in the one-dimensional Gray-Scott model*. Nonlinearity **10** (1997), 523–563.
- [ 7 ] Lee K.J., McCormick W.D., Pearson J.E. and Swinney H.L., *Experimental observation of self-replicating spots in a reaction-diffusion system*. Nature **369** (1994), 215–218.
- [ 8 ] Lee K.J. and Swinney H.L., *Lamellar structures and self-replicating spots in a reaction-diffusion system*. Phys. Rev. E **51** (1995), 1899–1915.
- [ 9 ] Doedel E.J., Champneys A.R., Fairgrieve T.F., Kuznetsov Y.A., Sandstede B. and Wang X., *AUTO97: Continuation and bifurcation software for ordinary differential equations (with HomCont)*. <ftp://ftp.cs.concordia.ca/pub/doedel/auto>, (1997).
- [10] Gray P. and Scott S.K., *Autocatalytic reactions in the isothermal, continuous stirred tank reactor: oscillations and instabilities in the system  $A + 2B \rightarrow 3B$ ,  $B \rightarrow C$* . Chem. Eng. Sci. **39** (1984), 1087–1097.
- [11] Kuznetsov Y.A., *Elements of Applied Bifurcation Theory*. Applied Mathematical Sciences **112**, Springer-Verlag.
- [12] Nishiura Y. and Ueyama D., *A Skeleton Structure of Self-replicating Dynamics*. Hokkaido University preprint series in mathematics. No.396 (1997), submitted for publication Physica D.

Department of Mathematics  
Faculty of Science  
Hiroshima University  
Higashi-Hiroshima 739-8526, Japan  
E-mail: daishin@math.sci.hiroshima-u.ac.jp